University of Mohamed Khider Biskra
Science and Technology
Department of mechanical engineering

# MASTER Dissertation

**Domain: Sciences and Technology**
**Field: Mechanical Engineering**
**Specialty: Energetic**

Ref.:.....

---

Presented by:
**Hichem Gherbia and Hamza Lazreg**

in Tuesday June 11, 2024

# Experimentalstudy of thermal performances of a solar collector with shape under the absorber

---

**Jury:**

| | | | | |
|---|---|---|---|---|
| Pr. | Fouad Chabane | Pr | University of Biskra | President |
| Pr. | Noureddine Moummi | Pr | University of Biskra | Supervisor |
| Pr. | Adnane Labed | Pr | University of Biskra | Examiner |
| Dr | Amira Hecini | Dr | University of Biskra | Aissistent Supervisor |

College year: 2023-2024

## Dedicase :

عائلتي العزيزة، لا يمكنني إيجاد الكلمات التي تعبر بالدقة عن مدى امتناني لكم ولكل الجهود التي بذلتموها من أجلي. كانت لي لحظات صعبة على مدى سنوات الدراسة، لكنكم كنتم دائماً حجر الزاوية الذي لجأت إليه في اللحظات الصعبة، وشمعة الأمل التي أضاءت لي الطريق في الظلام .

من خلال دعمكم اللامتناهي وتشجيعكم المستمر، استطعت أن أتغلب على التحديات وأتخطى الصعوبات التي واجهتني في رحلتي الأكاديمية. كانت كلماتكم الدافئة وحضوركم الدائم يعطياني القوة والثقة للمضي قدماً، وأنا ممتن بشدة لكل لحظة قضيتموها معي.

لقد كنتم الركن الأمن الذي تأملت فيه في أصعب اللحظات، والمصدر الذي أستمد منه الطاقة والإلهام لتحقيق أحلامي. واليوم، بفضلكم، أقف على مشارف التخرج، محققاً الهدف الذي طالما حلمت به. أهدي هذا الإنجاز الكبير لكم بكل فخر وامتنان، وآمل أن أكون دائماً عند حسن ظنكم وأن أجعلكم فخورين بي. شكراً لكم على كل شيء، وأتطلع إلى مشاركة المزيد من الإنجازات واللحظات الجميلة معكم في المستقبل.

## Acknowledgements :

بكل تواضع وامتنان، نتقدم بالشكر للبروفسور المؤطر نورالدين مومي على إرشاده الثمين ودعمه المستمر خلال فترة تخرجنا. كانت إرشاداته القيمة ومساندته الدائمة أحد أسباب نجاحنا. كما نود أن نعبر عن شكرن اللبروفسور فؤاد شعبان على مساعدته الكبيرة وتوجيهاته القيمة التي ساهمت في تطوير مهاراتنا وتحقيق أهدافنا الأكاديمية. ولايمكننا نسيان دورالطالبة الدكتوراه أميرة حسيني التي قدمت لنا الدعم والتشجيع المستمر، فلها كل الشكر والتقديرعلى تفانيها في مساعدتناعلى طول هذها لرحلة التخرجية.

**الملخص:**

يهدف البحث المعروض في هذه المذكرة إلى تحقيق أقصى كفاءة حرارية ممكنة من خلال استخدام حواجز مستطيلة موضوعة بشكل عمودي على تدفق المائع في مجرى التيار. تتمثل أهداف الدراسة في تقليل الضياع في الطاقة وزيادة الكفاءة الحرارية عبر تنفيذ تجارب متعددة باستخدام تنوع في عدد الحواجز. تم اختيار أربعة أوضاع مختلفة، والتي تتضمن مجموعة متنوعة من الحواجز، مع الحواجز النهائية في الوضع الرابع تضمن ستة حواجز. تركز الدراسة على تحديد معاملات التبادل الحراري وأرقام نسلت المحلية لتقييم الأداء الحراري لكل حالة. تم أيضًا حساب درجة حرارة الهواء عبر المجرى بناءً على درجات حرارة الأسطح المعنية. تم تنفيذ التجارب بتغيير معدلات التدفق الكتلي للمائع لتقييم تأثيرها على الأداء الحراري. بناءً على النتائج، تم التوصل إلى أن الوضع الرابع يعطي أعلى كفاءة حرارية بتدفق كتلي يبلغ 0.033 كغ/ثانية. وقد تم تطوير نموذج رياضي لوصف العلاقة بين رقم نسلت ومعاملات التبادل الحراري ومعلمات التجربة. تبرز الدراسة أهمية تحسين الكفاءة الحرارية من خلال استخدام الحواجز في مجرى التيار ودراسة العلاقات بين المتغيرات المختلفة المعنية بالأداء الحراري .

**الكلمات المفتاحية:** التبادل الحراري، رقم نسلت، الحواجز، التدفق، المجمع الشمسي، الكفاءة الحرارية.

## Abstract

The research presented in this memorandum aims to achieve maximum thermal efficiency byutilizing rectangular barriers placed vertically on the fluid flow in the stream channel. The objectives of the study include reducing energy loss and increasing thermal efficiency through conducting multiple experiments using variations in the number of barriers. Four different configurations were selected, each involving a variety of barriers, with the final configuration in the fourth mode consisting of six barriers. The study focuses on determining the heattransfer coefficients and local Nusselt numbers to assess the thermal performance of each case. Air temperature within the channel was also calculated based on relevant surface temperatures. The experiments were conducted by varying the mass flow rates of the fluid to evaluate their effect on thermal performance. Based on the results, it was found that the fourth mode yields the highest thermal efficiency at a mass flow rate of 0.033 kg/s. A mathematical model was developed to describe the relationship between Nusselt number and heattransfer coefficients and experimental parameters.

The study highlights the importance of enhancing thermal efficiency through the use of barriers in the stream channel and investigating the relationships between various variables relevant to thermal performance.

**Keywords:** heat exchange coefficients, Nusselt numbers, barriers, mass flow rate, solarcollector, thermal efficiency.

**Résumé :**

# ABSTRACT

Le travail présenté dans ce mémoire de fin d'études vise à atteindre une efficacité thermique maximale en utilisant d'obstacles (chicanes) rectangulaires placées verticalement dans l'écoulement du fluide dans un canal. Les objectifs de l'étude comprennent la réduction des pertes d'énergie et l'augmentation de l'efficacité thermique en réalisant plusieurs expériences en variant le nombre de chicanes. Quatre configurations différentes ont été sélectionnées, chacune impliquant une variété d'ostacles dont la configuration finale en mode quatre consistant en six chicanes. L'étude se concentre sur la détermination des coefficients de transfert de chaleur et du nombre de Nusselt local pour évaluer la performance thermique de chaque cas. La température de l'air à l'intérieur du canal a également été calculée en fonction des températures de surfaces. Les expériences ont été menées en faisant varier les débits massiques du fluide pour évaluer leur effet sur le rendement. Sur la base des résultats, il a été constaté que le quatrième mode produit la plus haute efficacité thermique pour un débit massique de 0,033 kg/s. Un modèle mathématique a été développé pour décrire la relation entre le nombre de Nusselt, les coefficients de transfert de chaleur et les paramètres expérimentaux.

L'étude met en évidence l'importance d'améliorer l'efficacité thermique grâce à l'utilisation de chicanes dans le canal d'ecoulement et d'explorer les relations entre diverses variables pertinentes pour la performance thermique.

**Mots clés :** échange thermique, nombres de Nusselt, chicanes, débit, capteur solaire, efficacité thermique

## NOMENCLATURE

A: Flow Rate (Kg/s).

c: The Speed of light [m/s].

CDER: centre for the development of Renewable Energies.

Cp: Specific heat of air (J/kg·°C).

Dh: Hydraulic diameter (m).

Ds: seasonal differences.

E: Energy [ J ].

FM: the Time zone number.

g: Acceleration due to gravity ($m/s^2$).

G: Global radiation ($W/m^2$).

h: Planck's constant (h=6.26*10^-37) [j/s].

HL: legal Time [h].

$i_0$: The annuel average [$w/m^2$].

J: The number of days in a year.

L: Channel length (m).

$L_0$: longitude [h].

MST: Mean Solar Time.

$Nu_L$: Nusselt number.

Qu: Useful power (W).

S: Surface of the absorber plate ($m^2$ ).

T: Temperature (°C).

Tab: Absorber temperature (°C).

TC: civil Time (TSm).

TSV: true solar time.

UT: Universal Time.

V: Average fluid velocity (m/s).

Λ: Pressure loss coefficient (-).

ΔT: Variation in the temperature of the heat transfer fluid (°C).

ΔP: Pressure Drop (Pa).

α: Absorption coefficient (-).

ε: emissivity (-).

τ: Transmission coefficient (-).

η: Efficiency (%).

*LISTE of FIGURES*

***LISTE of TABLES***

# GENERAL INTRODUCTION

## General Introduction

Solar energy has emerged as a pivotal element in the global quest for clean, sustainable and renewable energy sources, with its broad potential and many advantages making it indispensable in the global energy framework. Algeria has abundant sunshine throughout the year and is uniquely placed to harness solar energy and benefit from its benefits. The country has high levels of solar radiation, making it an ideal candidate for solar power generation and providing an opportunity to diversify its energy portfolio while reducing reliance on fossil fuels.

In the field of solar energy, our research endeavors focus on examining the thermal performance of flat solar collectors designed for air. These collectors use various techniques to increase thermal efficiency, including expanding the total surface area for heat exchange and inducing turbulent flow. One such technique involves incorporating rectangular metal obstructions, referred to as baffles, mounted on the bottom flow plate of the collector. These barriers amplify the surface area available for heat transfer and facilitate efficient heat exchange.

Our investigation was designed to systematically address this goal. The manuscript is organized into distinct chapters, each of which contributes to a comprehensive understanding of the thermal performance of flat panel solar collectors.

The first chapter provides a thorough review of the literature, focusing on techniques used to enhance performance in flat panel solar collectors. This review lays the foundation for our empirical inquiry

Chapter two provides a comprehensive overview of solar energy use globally and provides insight into flat panel solar collectors.

In Chapter Three, we delve into the experimental setup, explain the configuration of the barriers studied and outline the measurement equipment used. This chapter provides the context needed to conduct experiments and obtain data on thermal performance.

Finally, the concluding chapter of our research includes a comparative analysis of various styles of flat panel solar collectors. By examining the thermal efficiency and heat exchange characteristics of each mode, we seek to determine the most efficient and effective design configuration.

# CHAPTER I:

# BIBLIOGRQPHIC STUDY

## I.1 Introduction

In this chapter, we will examine studies conducted by various scientists regarding solar energy collectors and assess their significance and impact.

## I.2 Bibliographic study

Many kinds of air sensors are constructed and evaluated. It stands out due to their arrangements; several writers have enhanced these performances:

### I.2.1 Addition of baffles

**F. chabane et al [1]**. The effectiveness of solar collector systems in delivering energy output depends on the optical and thermal characteristics of the collector itself. This research entails an experimental examination of the coefficients used for collector convection. The methodologies used for convection are explained here. First, the internal temperature characteristics of both the absorber plate and the bottom plate are measured, followed by the efficiency calculation. Subsequently, external temperature measurements are used including inlet and outlet temperatures and ambient convection temperatures, in addition to internal hot box measurements.

A typical flat-plate collector configuration comprises an absorber enclosed within an insulated box, coupled with transparent cover sheets, typically made of Plexiglas. The absorber commonly consists of a metal sheet possessing high thermal conductivity, such as galvanized metal, coated with a selective material to optimize radiant energy absorption while mitigating radiant energy emission. The insulation within the box serves to diminish heat losses from the back and sides of the collector (Duffie and Beckman, 1991).

Plexiglas emerges as a favorable material for glazing flat plate solar collectors owing to its capability to transmit approximately 90% of incident shortwave solar radiation. Various types of plastics may also serve as viable cover materials, as select variants exhibit resilience to ultraviolet radiation over prolonged durations. Polycarbonate rigid sheets, polycarbonate rigid films, and corrugated sheets represent plastic alternatives readily available in the market. The utilization of plastics offers advantages such as resistance to damage from hail or impact, as well as their lightweight and flexible nature (Poulikakos, 1994).

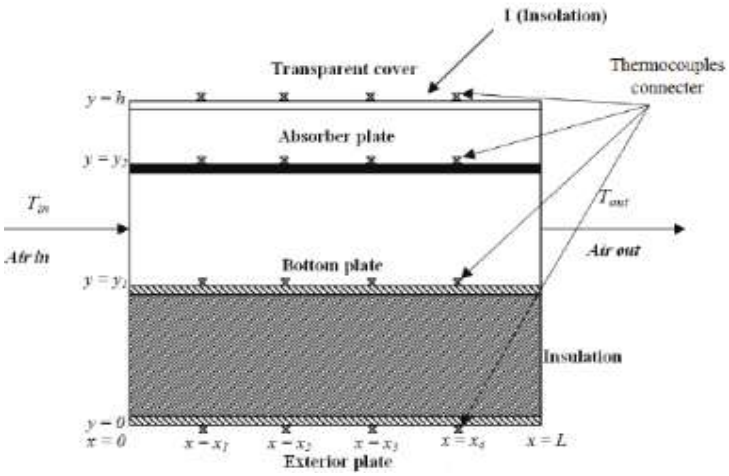


**Figure.I.1.** Flat plate solar air heaters.

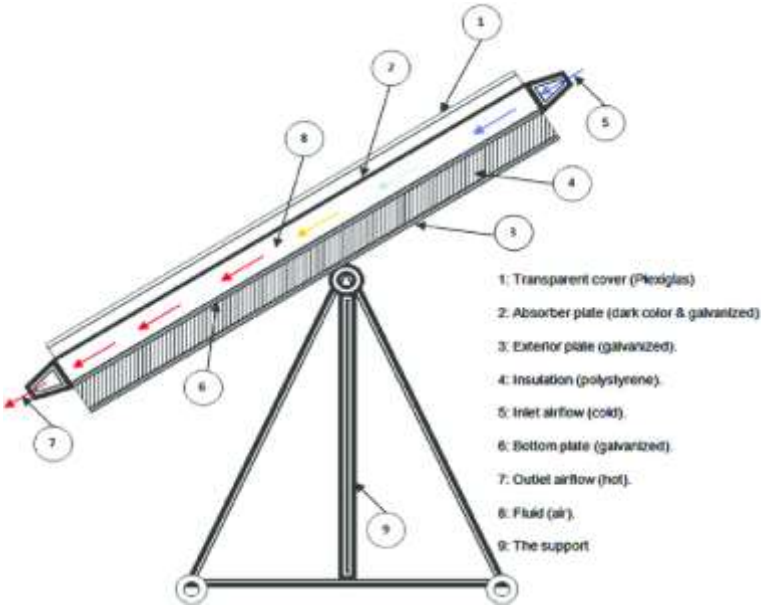


**Figure I.2.** Schematic view of the solar air collector.

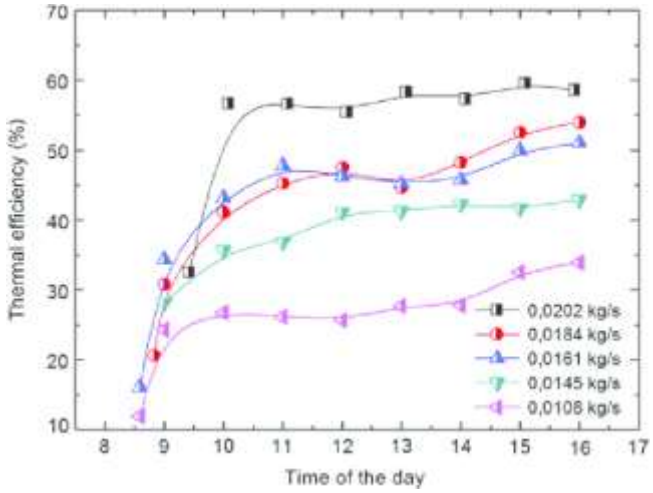


**Figure I.3.**Variation of collector efficiency at different mass flow rates.

**SachinSharma**, **RandipKumarDas and KishorKulkarni [2]:** Baffles have been extensively utilized within heat exchangers to augment performance [33–38]. Following a comprehensive review of the literature, it has been observed that the integration of ribs onto the heat-absorbing surface of a Solar Air Heater (SAH) has resulted in improved heat transfer. Researchers have also explored the substitution of ribs with baffles on the absorber surface, as baffles induce greater turbulence in the flow. To the authors' knowledge, sinusoidal wave-shaped roughened baffles have not been employed as obstacles on the absorber plate of a solar air heater. Consequently, identifying a research gap and seizing the opportunity to enhance the performance of rectangular SAH, sinusoidal wave-shaped baffles have been chosen for the present study. The perfoق current computational analysis aims to ascertain the optimal baffle shape that maximizes thermo-hydraulic performance (THP), while maintaining consistent geometric and operating parameters across all configurations.

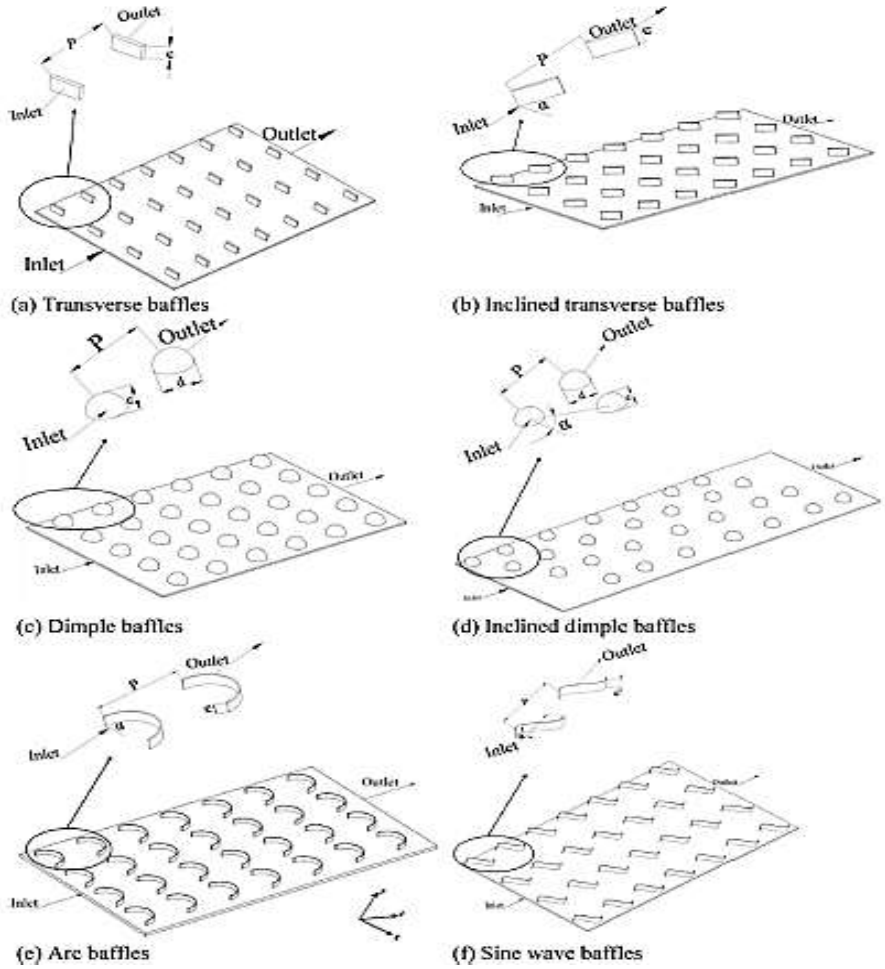


**Figure I.4.** Schematic view various baffles.

**Jerzy Szyszka, PieroBevilacqua and Roberto Bruno [3]:** The utilization of passive methodologies within building envelopes constitutes a significant stride towards attaining heightened efficiency and zero-energy benchmarks in construction. Trombe walls emerge as a compelling and feasible avenue for mitigating the energy demands of buildings, particularly in regions characterized by cold climates. This investigation presents a thorough experimental scrutiny of an innovative Trombe wall configuration termed the "thermo-diode Trombe wall," meticulously crafted to enhance energy efficiency by furnishing a judicious level of insulation for the building envelope. Such architectural design becomes imperative in frigid climates to curtail thermal losses while concurrently augmenting solar thermal influx into the interior spaces. An empirical study was undertaken from December through March, encompassing the continuous monitoring of external meteorological conditions alongside the principal thermal parameters, aimed at evaluating the thermal efficacy of the proposed architectural solution. The findings underscored that, under solar irradiation, the thermo-diode Trombe wall facilitated significant natural convection within the air cavity, attaining temperatures surpassing 35 °C in the upper segment, thereby delivering consistent heat infusion into the indoor milieu, even during inclement weather and sustained well beyond daylight hours. Notably, the efficiency, relative to incident solar radiation, peaked at 15.3% during a sunlit winter day characterized by optimal insulation.

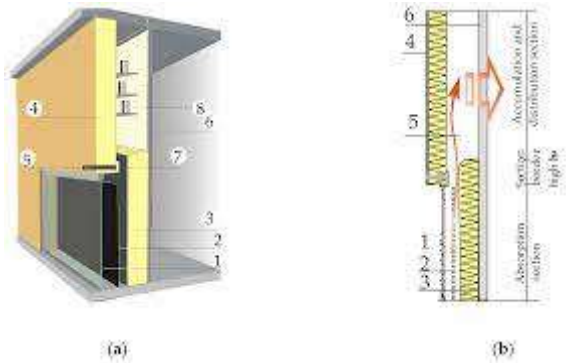

**Figure I.5.** Diagram of the TDTW operation in summer conditions: (**a**) general view and (**b**) cross-section of the wall (1—summer flap separator, 2—vent channel, 3—lockable infiltration channel, and 4— ventilation hole located on the room of the building).

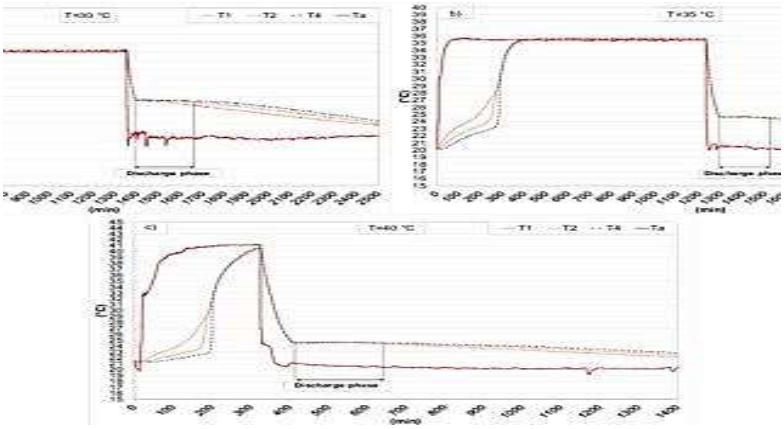

**Figure I.6.** Temperature measurements along the radial direction of the PCM containerduring the tests on the c with set-point temperatures of 30 °C (**a**), 35 °C (**b**), and 40 °C (**c**).

### I.2.2. Minimization of thermal losses:

**Donation Njomo [4]**: A mathematical model was developed to calculate thermal losses. The equations within this model were solved iteratively, and the resulting outcomes exhibited favorable agreement with empirical relationships documented in the literature. This investigation corroborated that the coefficient of thermal losses escalates with heightened emissivity of the absorber and its temperature, as well as with the convective exchange coefficient with the ambient air. Conversely, the coefficient of thermal losses diminishes with an increase in the distance between the absorber and the window. Moreover, it was observed that the coefficient of thermal losses increases with augmented emissivity of the absorber, its temperature, and the convective exchange coefficient with the ambient air, while concurrently decreasing with an increase in the distance between the absorber and the window.

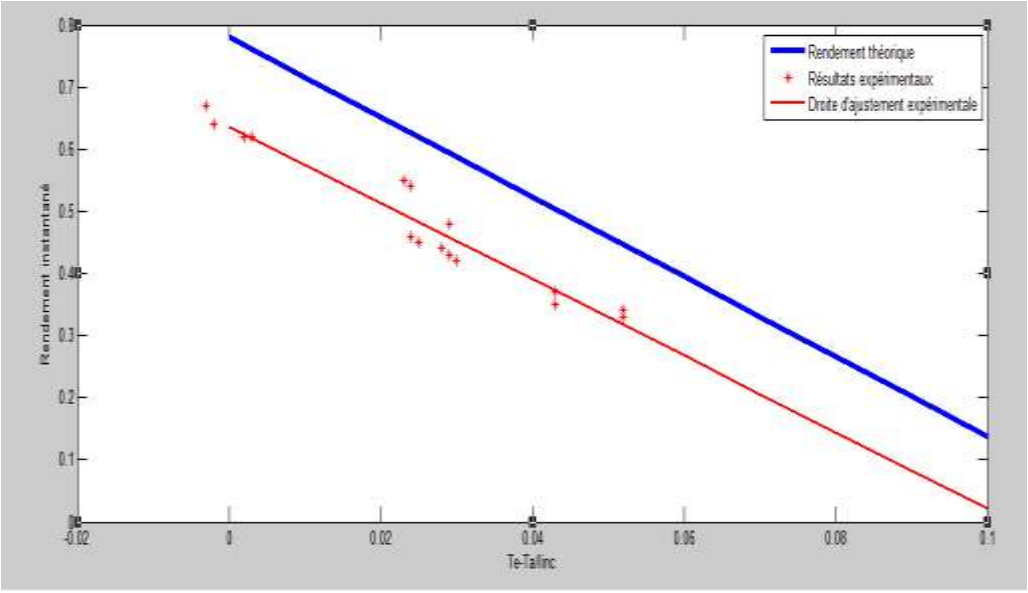


**Figure I.7.** Variation du rendement théorique et expérimental.

### I.2.3. Top of form:

**R. Kaoulal et al [4]:**A theoretical investigation was conducted on a single-pass flat solar air collector positioned between the absorber and the glazing, integrated into a facade, and designed for heating purposes, operating under dynamic natural convection conditions. The study aimed to determine temperature profiles of the glazing, absorber, and heat transfer fluid (air) at the outlet of the collector, as well as instantaneous thermal efficiency, achieved by solving heat balance equations using the nodal method.

To explore the influence of certain parameters on the coefficient of thermal losses towards the front of the flat solar collector, a mathematical model was devised using the methodology outlined in Chapter 1, based on the experimental plan established by mathematicians. This model, which is polynomial in nature, enables the calculation of these thermal losses. The equations of this model were solved iteratively utilizing MATLAB simulation.

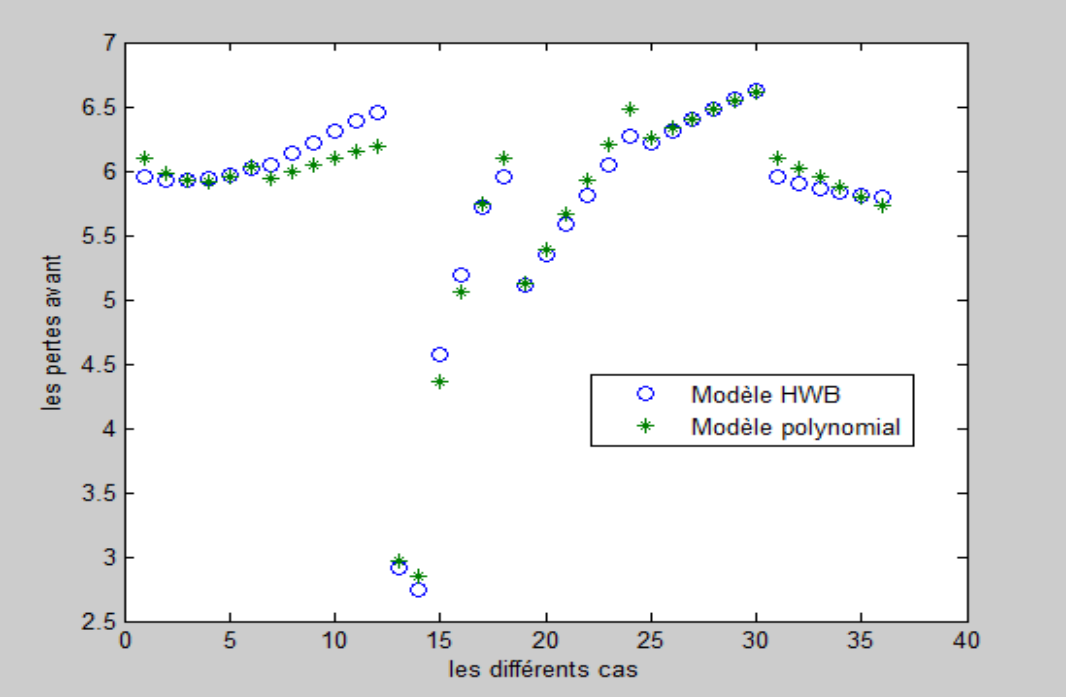


**Figure I.8.** Variation of losses before given by the theoretical model and the Multi-polynomial model.

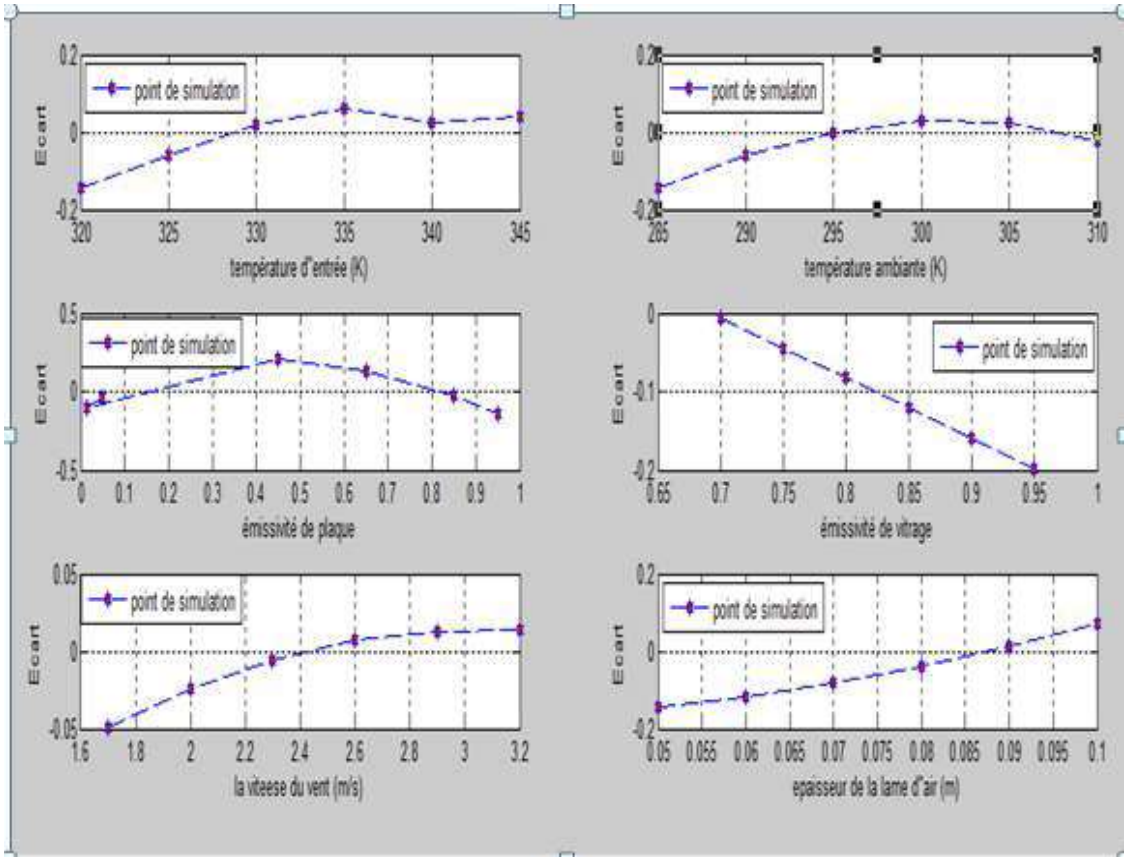


**Figure I.9.** Variation of the differences between the theoretical model and multi-polynomial model for the different parameters.

### I.2.4. Effect of heat carrier geometry on the thermal performance of solar collectors:

In the realm of solar collectors, the heat transfer fluid can traverse paths beneath, above, or alongside the absorber. Researchers have conducted numerous studies aimed at comprehending the impact of these fluid pathways on thermal losses. These investigations delve into how the shape and orientation of these pathways influence the overall heat transfer dynamics and resultant losses within solar collector systems.

### I.2.5. Collectorwith baffle :

**DonggenPeng, Xiaosong Zhang, Hua Dong and KunLv [5]:** The pin-fin array solar air collectors were equipped with a single, high-transmittance glazing measuring 4 mm in thickness and having dimensions of 1100 x 580 mm. This glazing served to minimize convective and long-wave losses to the atmosphere. Thermal losses to the environment from the sides and bottom of the collector were mitigated through effective thermal insulation, utilizing 50 mm and 70 mm polystyrene sheets, respectively.

The absorber within the pin-fin array solar air collectors comprised a 1 mm thick blackened stainless-steel sheet measuring 490 x 990 mm, integrated with iron pin-fins of 4 mm diameter

embedded within the flat plate. These features are illustrated in Figures 1 and 2, where metal pin-fins, absorber, and thermal insulation (benzene) are denoted by 'a', 'b', and 'c', respectively. The pin-fins varied in length from 10 to 45 mm and in span from 12 to 28 mm, resulting in the formation of 25 distinct configurations of novel solar collectors marked with PZ(s/d) (h/d).

The absorber and pin-fins were coated with a layer of black lacquer to enhance absorption of shortwave solar radiation passing through the transparent glazing, thus converting it into thermal energy to heat the absorber and pin-fins. A 50 mm gap separated the glazing from the absorber plate. Solar radiation absorbed by the absorber was convectively transferred to the air stream, which entered from the bottom and ascended across the absorber. A fan situated at the bottom of the collector facilitated the upward flow of air, distributing it evenly over the entire column area of the collector. This airflow direction, driven by the fan, aligned with natural convection driven by buoyancy, thereby enhancing the thermal performance of the collectors.

The pin-fin array solar air collector was mounted on a stainless-steel board measuring 1100 x 600 x 140 mm, affixed to a bracket soldered with L40 x 4 angle iron, allowing for adjustment of the collector's inclination. An advantage of this collector design is its flexibility in geometry, size, and material selection, within commercially available ranges. Air temperature rises were measured using shielded thermocouples installed at the inlet and outlet of the collector. Each channel of the data logger was equipped with a separate amplifier and calibrated using a thermostat and calibration thermometer to ensure precision within ±0.2°C. Air volume flow rates were determined with an accuracy of ±3% using an orifice plate positioned at the front of the collector. Solar irradiation heat flux was measured with a pyranometer, providing accuracy within ±3%.

**Figure I.10.** Photograph of examined solar air collector in the experimental site. Right : Photographe of test and data acquisition system.

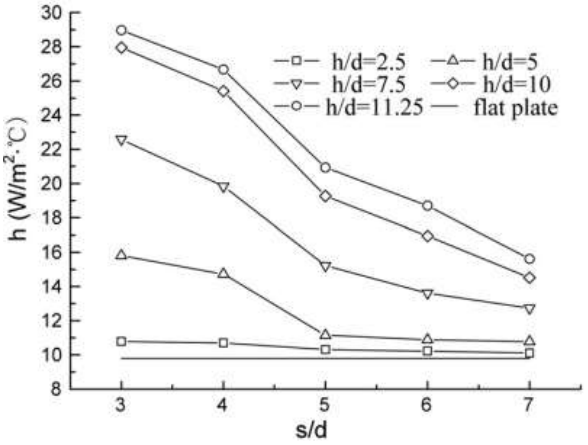


**Figure I.11.** Heat transfer coefficients of pin-fin and flat-plate collectors.

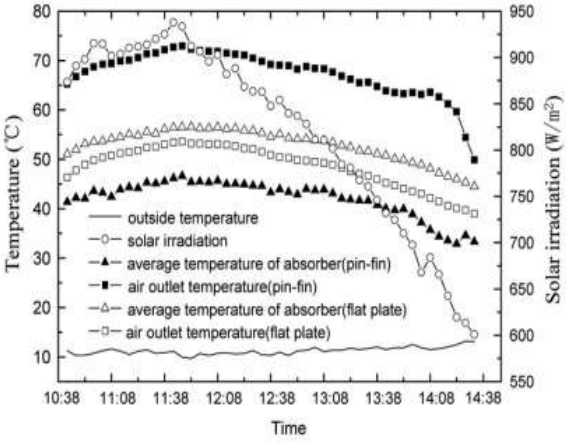


**Figure I.12.** Thermal conditions of two kinds of collectors (flat plate and PZ3-11.25).

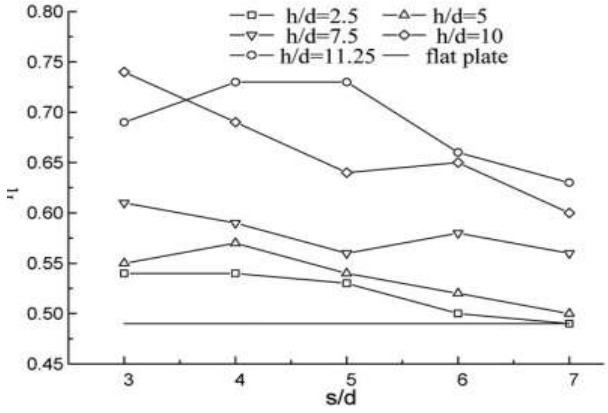


**Figure I.13.** Experimental efficiencies of pin-fin and flat-plate collectors.

**Table I.1:** Efficiency equations on 26 kinds of collectors:

| Type | Efficiency Equation | Type | Efficiency Equation |
|---|---|---|---|
| **PZ3-2.5** | $\eta=0.526-2.59*(T_{a,i}-T_0)/I_C$ | PZ4-2.5 | $\eta=0.52-2.64*(T_{a,i}-T_0)/I_C$ |
| **PZ3-5** | $\eta=0.563-2.85*(T_{a,i}-T_0)/I_C$ | PZ4-5 | $\eta=0.557-2.82*(T_{a,i}-T_0)/I_C$ |
| **PZ3-7.5** | $\eta=0.619-3.01*(T_{a,i}-T_0)/I_C$ | PZ4-7.5 | $\eta=0.594-2.98*(T_{a,i}-T_0)/I_C$ |
| **PZ3-10.5** | $\eta=0.682-3.1*(T_{a,i}-T_0)/I_C$ | PZ4-10.5 | $\eta=0.675-3.08*(T_{a,i}-T_0)/I_C$ |
| **PZ3-11.25** | $\eta=0.716-3.11*(T_{a,i}-T_0)/I_C$ | PZ4-11.25 | $\eta=0.702-3.07*(T_{a,i}-T_0)/I_C$ |
| **PZ5-2.5** | $\eta=0.515-2.62*(T_{a,i}-T_0)/I_C$ | PZ6-2.5 | $\eta=0.507-2.6*(T_{a,i}-T_0)/I_C$ |
| **PZ5-5** | $\eta=0.532-2.65*(T_{a,i}-T_0)/I_C$ | PZ6-5 | $\eta=0.529-2.66*(T_{a,i}-T_0)/I_C$ |
| **PZ5-7.5** | $\eta=0.582-2.84*(T_{a,i}-T_0)/I_C$ | PZ6-7.5 | $\eta=0.569-2.7*(T_{a,i}-T_0)/I_C$ |
| **PZ5-10.25** | $\eta=0.65-2.96*(T_{a,i}-T_0)/I_C$ | PZ6-10.25 | $\eta=0.637-2.9*(T_{a,i}-T_0)/I_C$ |
| **PZ5-11.25** | $\eta=0.68-2.99*(T_{a,i}-T_0)/I_C$ | PZ6-11.25 | $\eta=0.669-2.94*(T_{a,i}-T_0)/I_C$ |
| **PZ7-2.5** | $\eta=0.5-2.61*(T_{a,i}-T_0)/I_C$ | | |
| **PZ7-5** | $\eta=0.52-2.62*(T_{a,i}-T_0)/I_C$ | | |
| **PZ7-7.5** | $\eta=0.562-2.75*(T_{a,i}-T_0)/I_C$ | Flat-plate | $\eta=0.502-2.56*(T_{a,i}-T_0)/I_C$ |
| **PZ7-10.5** | $\eta=0.619-2.82*(T_{a,i}-T_0)/I_C$ | | |
| **PZ7-11.25** | $\eta=0.642-2.986*(T_{a,i}-T_0)/I_C$ | | |

In their study**, T. Rajaseenivasan and K. Srithar [6]** examine both the practical implementation and theoretical underpinnings of a solar still. They conduct experiments involving the integration of circular and square fins, crafted from mild steel pipes, into the basin of the solar still. To evaluate the system's performance comprehensively, they manipulate the water depth at levels of 1 cm, 2 cm, 3 cm, and 4 cm, and utilize various wick materials to cover the fins.

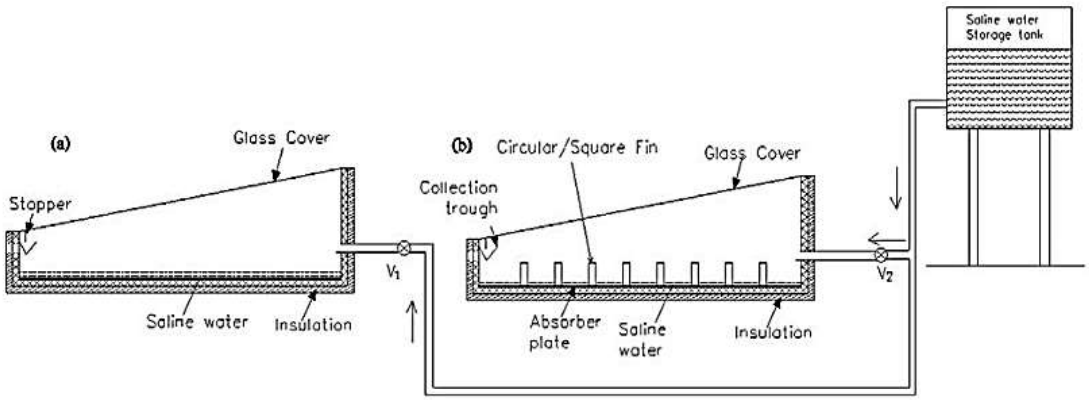


**Figure I.14.** Schematic view of solar stills. (a) Conventional still, (b) modified still.

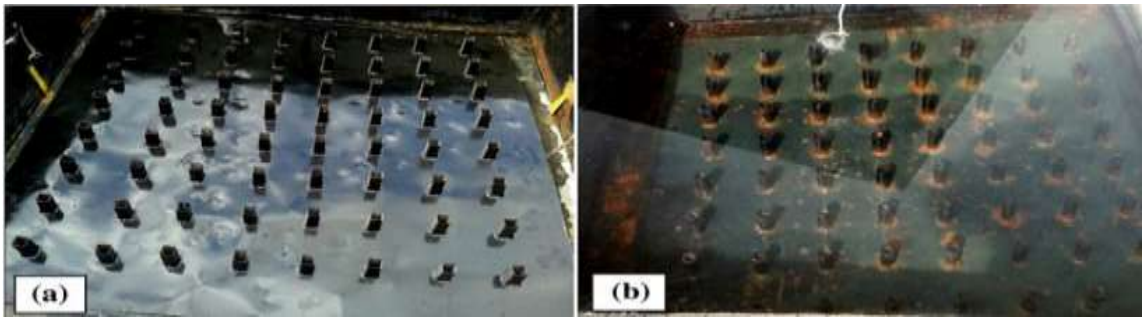


**Figure I.15.** (a) Square finned basin. (b) Circular finned basin.

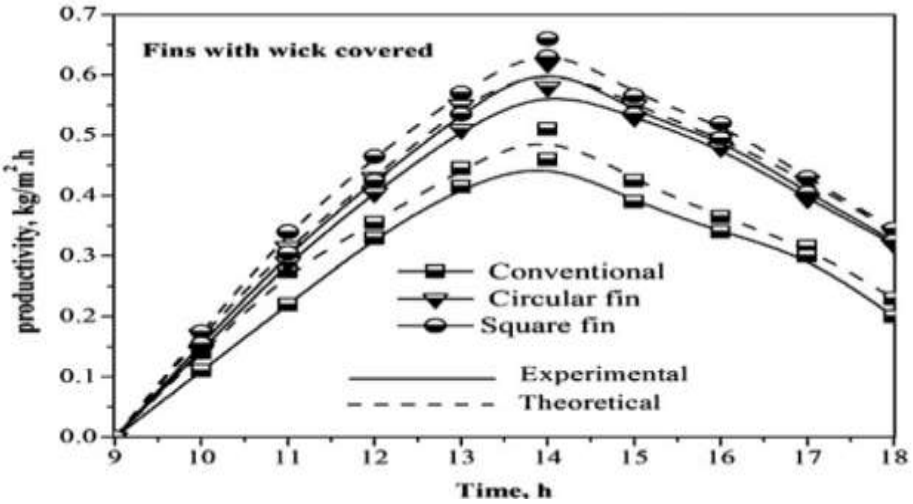


**Figure I.16.**Performance of solar still for fins covered with wick material.

### I.2.6. Solar collect or with double passes without and with a porous medium:

**K. Sopian, Supranto, W.R.W. Daud, M.Y. Othman, and B. Yatim [7]:** The solar simulator employs 45 halogen lamps, each rated at 300 W, with the capability of achieving a maximum average radiation of 600 W/m^2. Dimmers are utilized to control the amount of radiation received by the test collector, with the capacity to adjust the radiation intensity down to 558 K.

The collector configuration comprises a glass cover, an insulated container, and a black-painted aluminum absorber. Its dimensions measure 120 cm in width and 240 cm in length. Airflow is directed through two channels within the collector: initially through the first channel, formed by the glass covering the absorber plate, and subsequently through the second channel, formed by the back plate and the absorber plate. The depths of both channels can be adjusted to optimize operational efficiency. The inlet temperature to the collector is regulated by heating the inlet air.

Data recording is facilitated by a Yokogawa HR 1300 recorder, capturing essential parameters such as temperatures (inlet, outlet, absorber, glass cover, and ambient) and the intensity of the solar simulator. Type-K thermocouples are utilized for temperature measurement, while solar intensities are recorded using a pyranometer. Additionally, an Airflow LCA 6000 instrument is employed to measure the linear velocity of airflow. Mass airflow rates are calculated under the assumption of an ideal gas. The schematic representation of the indoor testing facility and the experimental setup of the double-pass solar collector are depicted in Fig. 1, with Fig. 2 illustrating the cross-section of the collector incorporating porous media.

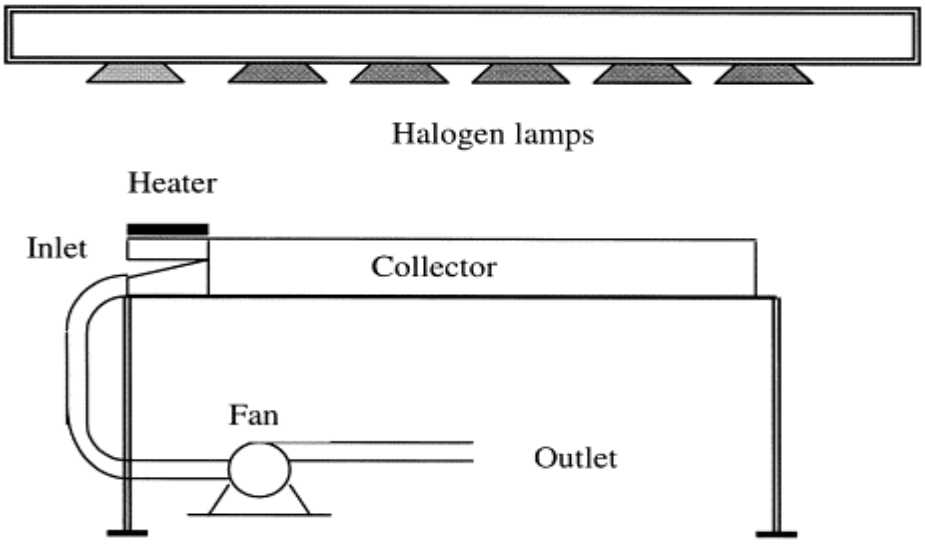


**Figure I.17.** Indoor testing facility of double-pass solar collector

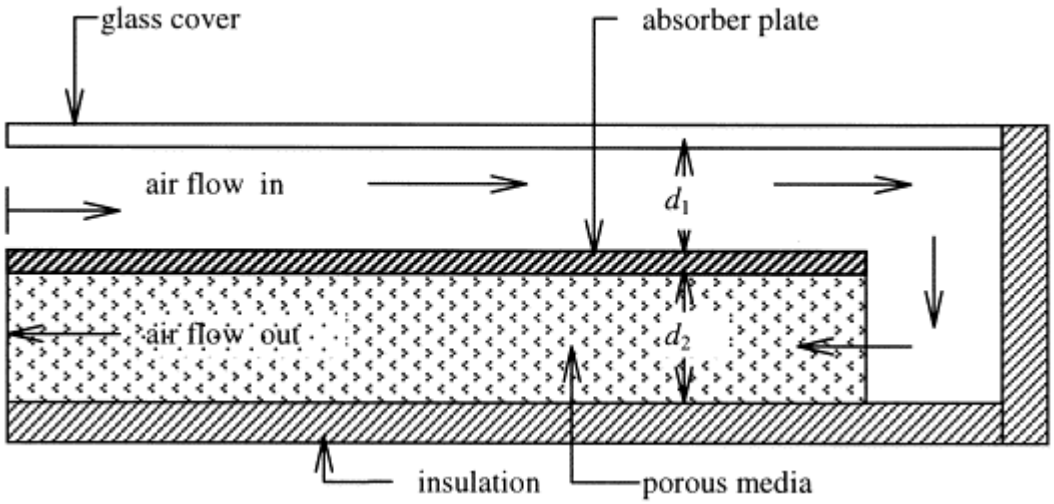


**Figure I.18.** The schematic of a double-pass thermal solar collector with porous media in the second channel.

### I.2.7. solar collector that employs a metal mesh:

**Chii-Dong Ho, Chun-Sheng Lin, Tz-Jin Yang and Chun-Chieh Chao [8]:** A novel device has been created to introduce an absorber plate, dividing a flat-plate channel into two subchannels, enabling double-pass wire mesh packed operations. This wire mesh packed device significantly enhances heat transfer efficiency compared to both flat-plate single-pass and double-pass operations using identical working dimensions. The performance of the device was investigated through both experimental and theoretical means. Remarkably, there was a substantial agreement between the theoretical predictions and the measured values obtained from experimental results. Notably, employing wire mesh packed double-pass operations beneath the absorber plate, especially with external recycling, led to considerable improvements in heat transfer. Additionally, the effects of recycle ratio on heat transfer efficiency and the increase in power consumption were thoroughly discussed.

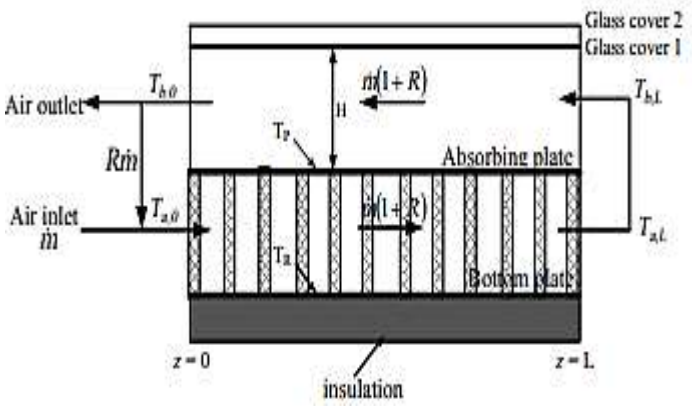


**Figure I.19.** A schematic drawing of a wire mesh packed double-pass solar air heater.

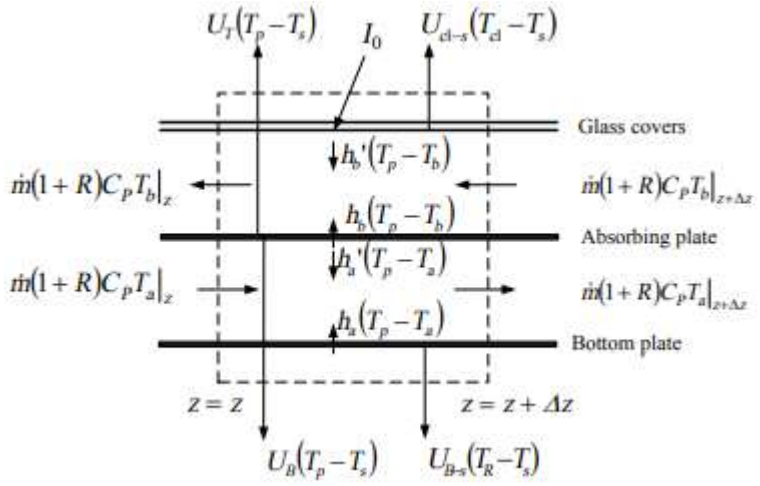


**Figure I.20.** The energy balance on energy flow within a finite fluid element.

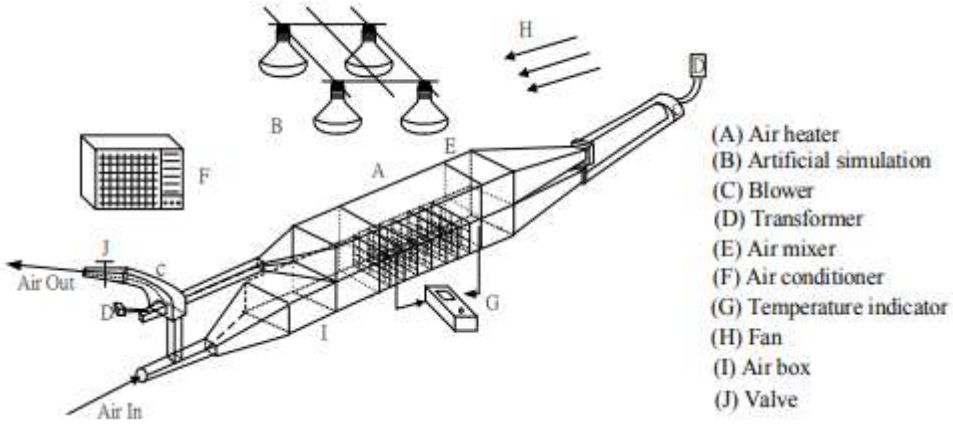


**Figure I.21.** Experimental setup of a wire mesh packed double-pass solar air heater.

The ambient temperature (Ts = (30 ± 0.1) °C) was maintained using an air conditioner and monitored at a position 0.15 m above the outer glass cover. During experimental runs, a fan (EUPA TSK-F1426, 14" EUPA, Xiamen, Fujian, China) provided a steady airflow of 1.0 m/s. Temperatures at the inlet and outlet of the solar collector, as well as the temperature of the absorber plate, were recorded using thermocouples (TFC-305A, Hwa Tai Technology Co., Ltd., Taipei, Taiwan). The ambient air was supplied consistently by a blower (Teco 3 Phase Induction Motor, Model BL model 552, Redmond Co., Owosso, MI, USA), with the flow rate controlled by a transformer and measured using an anemometer (Model 24-611, Kanomax Japan Inc., Osaka, Japan).

Prior to entering the lower subchannel, the airflow with mass flow rate m and temperature Tin was mixed with the airflow exiting from the upper subchannel with mass flow rate Rm and

temperature Tb,0. This mixing process was regulated by a valve located at the end of the lower subchannel.

A set of 14 adjustable radiation sources, each rated at 110 V and 125 W, was utilized, controlled by a set of on/off switches, to simulate incident solar radiation. The incident solar radiation (I0) was measured and recorded using a Model No. 455 pyranometer (TSI Inc., St. Paul, Shoreview, MN, USA).

### I.2.8. Influence of absorber geometry:

**M. CharishmaBrunda and PisipatySrinivas Kishore [9]:** Fossil fuels have become integral to our daily lives, serving as a primary source of energy. Despite this reliance, the importance of renewable energy resources, particularly solar energy, cannot be understated due to its abundant availability. Among various applications of solar energy, solar air heaters stand out as a crucial means of converting solar energy into thermal energy. These devices are known for their simplicity, affordability, and widespread usage in harnessing solar energy.

However, conventional solar air heaters often exhibit limited thermal performance, attributed to the relatively low heat transfer coefficient between the absorber plate and the carrier fluid (air). To address this limitation, extended surfaces, such as wavy fins, are commonly attached to the absorber plate to enhance thermal performance. The primary objective of this study is to enhance the efficiency of a solar flat plate collector by incorporating wavy fins onto the absorber plate, with a focus on augmenting heat transfer and improving overall efficiency.

Experimental investigations involve varying air mass flow rates ranging from 250 kg/hr to 350 kg/hr. It was observed that the effective heat transfer coefficient reached its maximum value at the highest air mass flow rate of 350 kg/hr. Additionally, the use of wavy fins resulted in lower friction factors and higher pressure drops, particularly at larger Reynolds numbers.

Analytical assessments were conducted to compare the thermal performance of conventional solar air heaters with those equipped with wavy fins. Based on the comparative analysis, recommendations are made for the optimal configuration of solar air heaters, particularly for applications such as drying processes.

**Priyam and Chand [9]:** Research findings have demonstrated the significant effectiveness of wavy fins in augmenting heat transfer within a solar air heater. The authors observed that the inclusion of wavy fins resulted in superior thermal performance compared to a smooth duct configuration. Specifically, the maximum enhancement in thermal efficiency and effective

efficiency attributable to wavy fins was found to be approximately 63.41% and 35.83%, respectively, relative to the smooth duct configuration.

**Karim and Hawlader [9]:** In an experimental study, the thermal performance characteristics of a solar air heater equipped with a V-corrugated absorber plate, designed for drying applications, were investigated. The analysis revealed that the incorporation of V-corrugations resulted in a 12% increase in efficiency compared to a flat plate absorber configuration. Additionally, a flow rate of 0.035 kg/m2s was recommended for drying applications, as it corresponded to higher levels of efficiency and outlet air temperature.

**Eshan Kumar Nashine, P.S.Kishore [9] :** A numerical investigation was conducted on a compound parabolic collector for the purpose of process steam generation. The performance analysis of the system revealed the potential for enhancing thermal efficiency up to 75%. This analysis was conducted considering two different locations, namely Visakhapatnam and Mumbai.

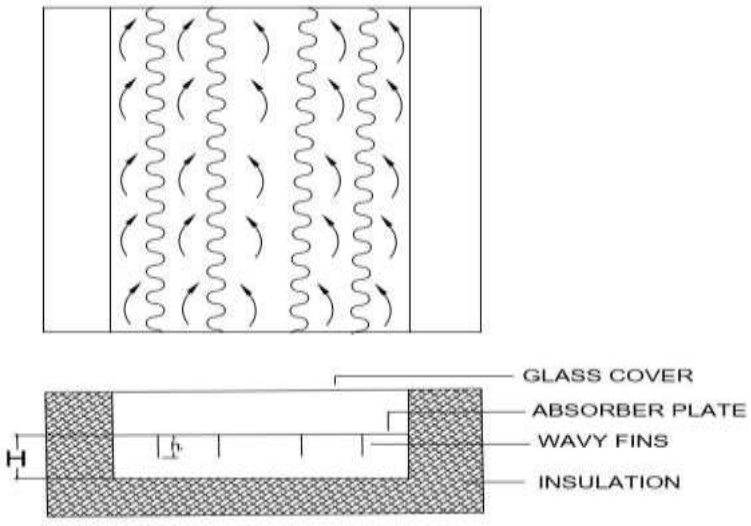


**Figure I.22.** Wavy finned Solar Air Heater.

## I.3. Conclusion

In conclusion, our comprehensive study on solar energy collectors, conducted by scientists, has revealed that the performance of these devices is predominantly influenced by their thermal and optical physical parameters. Consequently, numerous studies are underway to investigate each component of these systems in detail.

## 1.4. References

[1] Chabane, F., Moummi, N., Benramache, S., &Brima, A. (2013). Thermal efficiency analysis of a single-flow solar air heater with different mass flow rates in a smooth plate. *Frontiers in Heat and Mass Transfer (FHMT)*, *4*(1).

[2] Sharma, S., Das, R. K., &Kulkarni, K. (2021). Computational and experimental assessment of solar air heater roughened with six different baffles. *Case Studies in Thermal Engineering*, *27*, 101350.

[3] Szyszka, J., Bevilacqua, P., & Bruno, R. (2020). An innovative trombe wall for winter use: The thermo-diode trombe wall. *Energies*, *13*(9), 2188.

[4] Sopian, K., Daud, W. R. W., Othman, M. Y., &Yatim, B. (1999). Thermal performance of the double-pass solar collector with and without porous media. *Renewable energy*, *18*(4), 557-564.

[5]Peng, D., Zhang, X., Dong, H., &Lv, K. (2010). Performance study of a novel solar air collector. *Applied Thermal Engineering*, *30*(16), 2594-2601.

[6]Grira.F,'Improving Thermal performance of a solar collector without and with baffles'31 May 2017.

[7]Sopian, K., Daud, W. R. W., Othman, M. Y., &Yatim, B. (1999). Thermal performance of the double-pass solar collector with and without porous media. *Renewable energy*, *18*(4), 557-564..

[8] Ho, C. D., Lin, C. S., Yang, T. J., & Chao, C. C. (2014). Recycle Effect on Device Performance of Wire Mesh Packed Double-Pass Solar Air Heaters. *Energies*, *7*(11), 7568-7585.

[9] ''M.charishmaBrnda'',''PisIpatySrinivas Kishore'' ' Heat Transfer Enhancement of Wavy Finned Solar Air Heater'

# CH APTER II

# THEORETICAL STUDY

## II.1 Introduction

Solar thermal energy relies on harnessing the heat emitted by the sun. The solar radiation reaching a given surface depends directly on its orientation and the position of the sun. Accurate prediction of the sun's position enables optimal placement of solar collectors, as their productivity is maximized when exposed at an inclination and orientation dependent on their installation site. Thus, understanding the position of the sun over time is fundamental.

## II.2 The solar energy:

### II.2.1Origine:

The conditions residing at the core of the Sun conducive to the interaction of various hydrogen atoms lead to a thermonuclear fusion reaction. This process results in the fusion of four hydrogen nuclei to form a helium nucleus, accompanied by the emission of energy in the form of gamma and X-ray radiations.

Every second, 564 million tons of hydrogen are transformed into 560 million tons of helium. This difference of 4 million tons per second corresponds to the disparity in binding energy between hydrogen and helium protons, resulting in the release of energy in the form of radiation, estimated at 3.7 × 10^26 joules per second.

### II.2.2 Distinctive Characteristics:

**II.2.2.1. Solar energy constitutes the sole external source of energy for the Earth, exhibiting the following characteristics:**

• Universality: Its maximum power density is 1 kW/m² at noon under a clear sky across the entire planet.

• Diffusion: The maximum power density received at ground level (1 kW/m²) is low, qualifying it as diffuse energy.

• Abundance: Our planet receives over 10^4 times the energy consumed by humanity.

• Variability: Solar energy is intermittent and variable due to the alternation of day and night, as well as seasonal and daily variations in sunlight.

• Energy loss: The energy received by a given surface is not fully recoverable due to losses in conductive, convective, or radiative forms.

• Cleanliness: Solar energy is a clean source of energy.

### II.2.3 Capitation:

There are various techniques for harnessing a portion of this solar energy, notably...

#### II.2.3.1 Solar thermal Energy:

Solar thermal energy is a process of converting solar energy into thermal form, which can be utilized in various ways:

- Direct use of heat: solar water heaters, solar heating systems, solar cookers, and solar dryers.

- Indirect use where the heat is utilized for other purposes: solar thermal power plants, production of solar refrigeration.

#### II.2.3.2 Solar thermodynamic energy:

Solar thermodynamic energy harnesses solar thermal energy to generate electricity following the same principle as a conventional power plant but using Helios thermal power plants. Three main types of power plants are commonly used:

- Parabolic trough power plants, designed to reach temperatures between 300 and 350 °C.

- Parabolic dish power plants, intended to reach temperatures of 1000°C or higher.

- Solar tower power plants, designed to reach 1000 °C. **[1] [2]**

#### II.2.3.2 Photovoltaic solar energy:

It enables the production of electricity by transforming a portion of solar radiation using a photovoltaic cell **[1].** Photovoltaic cells employ the photovoltaic effect and are composed of a layer of semiconductor material and a semiconductor junction. Silicon is the most used material; however, gallium arsenide offers superior performance, albeit at a significantly higher cost **[1]**.

## II.3 Solar radiation:

The thermonuclear reactions occurring at the core of the Sun generate corpuscular and electromagnetic radiations that propagate in all directions through the interstellar vacuum at a velocity of3.10 m/s and covering all wavelengths from X-rays and gamma rays to R distant. This means that 99.9% of the energy is between 0.2 and 8µm **[1].**

With an acceptable approximation, it can be assumed that the sun radiates like a black body at a temperature of 5762 K, referred to as the apparent temperature of the sun, which does not correspond to the physical reality **[2].**

The distribution of solar energy across the bands of the thermal radiation spectrum is provided in Table II.1:

| **Wavelength ($\mu$m)** | **0-0.38** | **0.38-0.78** | **0.78** |
|---|---|---|---|
| **Percentage (%)** | 6.4 | 48 | 45.6 |
| **Energy (w/m2)** | 87 | 656 | 623 |

**Table II.1:** Spectral Distribution of Thermal Radiation **[3].**

Figure 4 illustrates solar radiation, its frequencies, and wavelengths.

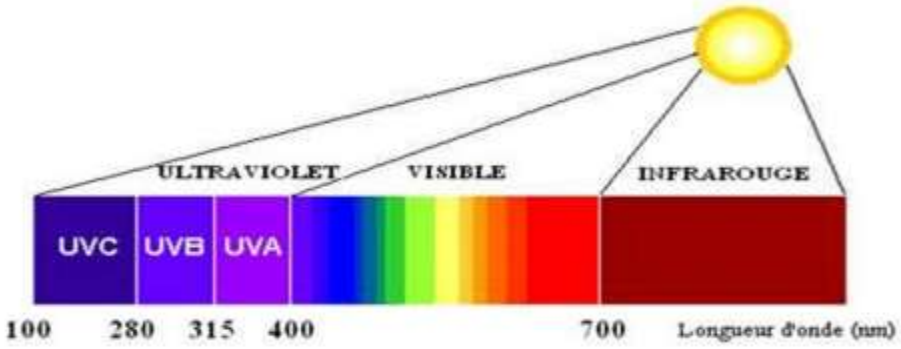


**Figure II.1** Solar Spectrum. **[1]**

### II.3.1 Ground-level solar irradiance or solar radiation:

It refers to the energy received over a certain period. Several main components are distinguished, namely:

#### II.3.1.1 Direct radiation (I):

This is direct radiation, which traverses the atmosphere without undergoing any modifications. It is received directly from the sun, without being diffused by the atmosphere, and its rays are parallel to each other

#### II.3.1.2 Diffuse radiation (D):

This is the component of solar radiation scattered by solid or liquid particles suspended in the atmosphere, such as air, clouds, aerosols, etc. This scattered radiation does not have a preferred direction.

#### II.3.1.3 Global radiation (G) :

This is the global component of solar radiation, which is the sum of direct and diffuse radiations **[4].**

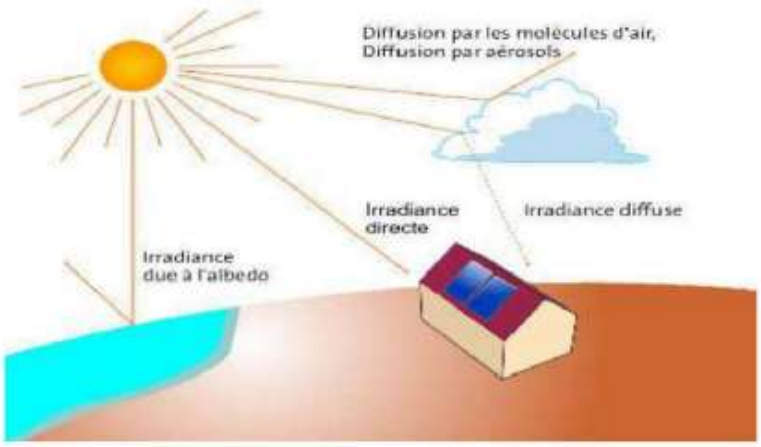


**Figure II.2** Components of solar radiation at ground level **[5].**

## II.4 Calculation of the position of the sun:

### II.4.1 Position parameters:

#### II.4.1.1 Earth coordinates:

All points on the Earth's surface can be identified by two coordinates, known as Earth coordinates, namely: latitude (φ) and longitude (L) **[6]**.

##### II.4.1.1.1 Longitude (L or λ):

It is the angle between the meridian of the location and the prime meridian (Greenwich, England), positive to the East and negative to the West. There are 23 meridians separated by 15°, giving rise to the 24 time zones.

##### III.4.1.1.2. Latitude (φ):

It allows to locate the angular distance of any point relative to the equator. It varies from 0° at the equator to 90° at the North Pole.

##### III.4.1.1.3 Altitude (z):

The altitude of a point corresponds to the vertical distance between that point and a theoretical reference surface (mean sea level).

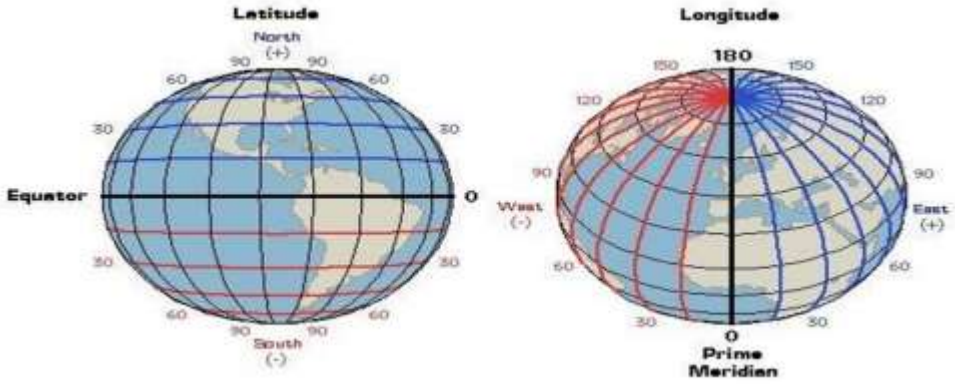


**Figure II.3.** Longitudes and latitudes on the globe **[7].**

### II.4.1.2 Equatorial coordinates:

#### II.4.1.2.1 Declination (δ):

The solar declination (δ) is the angle formed by the direction of the sun and the Earth's equatorial plane. This angle varies with the seasons from -23.45° to +23.45°.

Spring Equinox: March 21δ= 0°

Summer Solstice: June 22δ= +23,45°

Autumn Equinox 23 September δ= 0°

Winter Solstice 22 December δ= -23,45°

Between these 4 notable points, δ takes all intermediate values which can be calculated using the relationships **[8]:**

$$\delta = 23{,}45 \sin[\frac{360}{365}(284 + n)] \quad \textbf{(II.1)}$$

*Ou bien*

$$\delta = 23{,}45 \sin[\frac{360}{365}(n - 81)] \quad \textbf{(II.2)}$$

n: number of the day of the year counted from January 1st.

The variation of the solar declination throughout the year is depicted in Figure (I-10) **[9].**

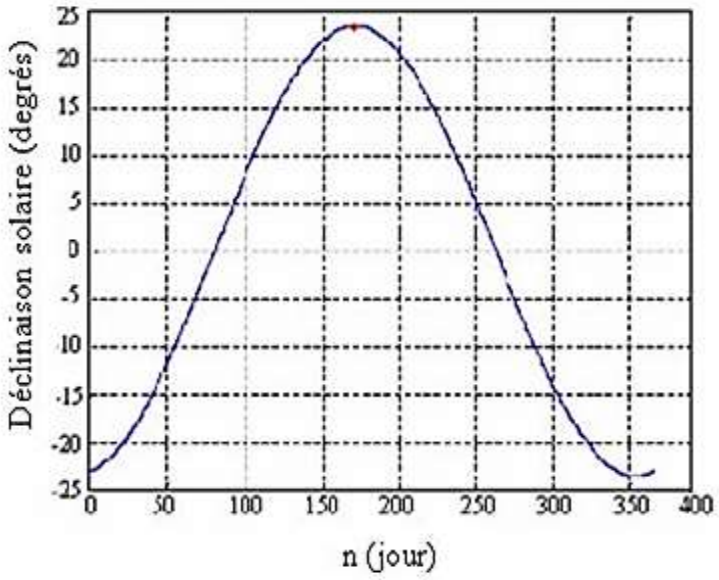


**Figure II.4** Solar declination as a function of the day number of the year, n.

**II.4.1.2.2 Hour Angle (ω or HA):**

It is the angle formed by the plane of the celestial meridian and the trajectory of the Earth/Sun direction on the plane of the celestial equator, or it is the angular displacement of the sun around the polar axis in its east to west motion relative to the local meridian. It is zero at solar noon, negative in the morning, and positive in the afternoon. It is given by **[6]:**

$$\omega = 15 * (TSV - 12) \quad \textbf{(II.3)}$$

ω: in degrees.

TSV: true solar time in hours.

Thus, an hour angle of 15° is equivalent to one hour of true solar time.

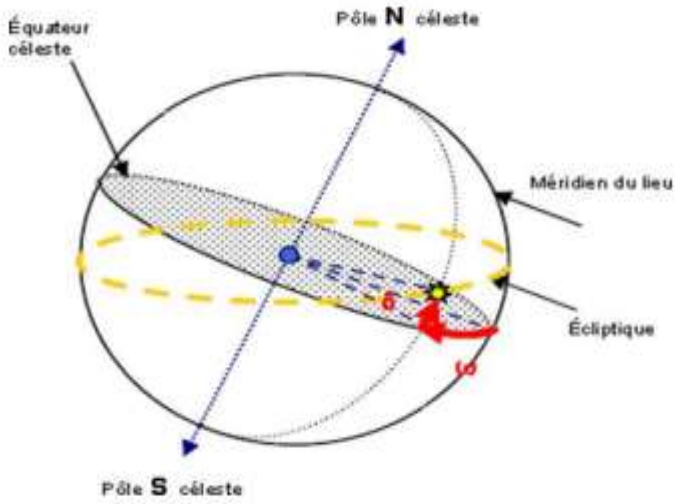


**Figure II.5** Hour angle coordinate system **[7].**

### II.4.1.3. Horizontal coordinates:

The position of a celestial body in space can be identified by its horizontal coordinates defined in the celestial sphere. The celestial sphere is the sphere with the Earth as its center and the distance between the Earth and the studied celestial body (the Sun in our case) as its radius.

These coordinates depend on the observing location and are also referred to as local coordinates **[6].**

#### II.4.1.3.1 Angular Height (h):

The angular height, also known as solar altitude, is the angle formed by the horizontal plane of the observation location and the direction of the celestial body. It is given by the trigonometric relation **[8]:**

$$\text{Sin } h = \sin \delta \sin \varphi + \cos\delta\cos\varphi\cos\omega \qquad \textbf{(II.4)}$$

#### II.4.1.3.2 Azimuth (a):

It is the angle between the meridian of the location and the vertical plane passing through the sun. It is measured positively towards the West.

The azimuth is related to the hour angle, the height, and the declination by the relation **[8]:**

$$\text{Sin } a = \sin \omega\cos\delta/\cos h \qquad \textbf{(II.5)}$$

And if one wishes to express the azimuth independently of the height h, one can use the formula:

$$\tan a = \sin \omega/ (\sin \varphi\cos\omega - \cos\varphi \tan \delta) \qquad \textbf{(II.6)}$$

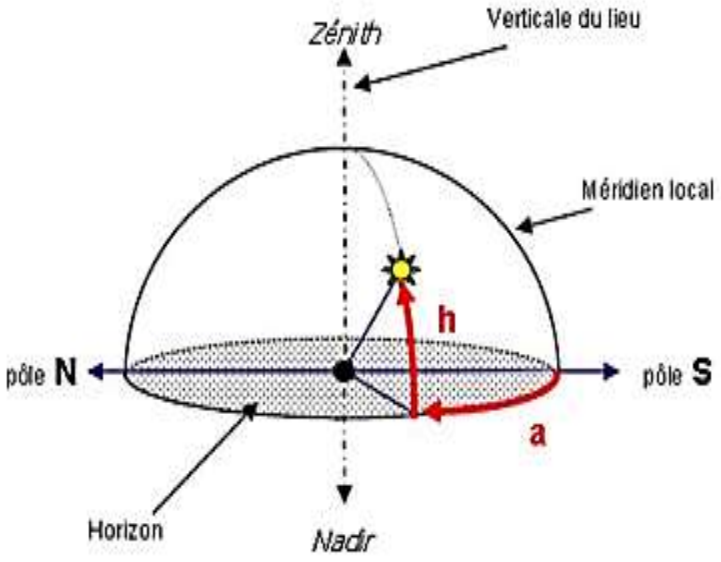


**Figure II.6** Height and azimuth for an observer in the Northern hemisphere **[7].**

## II.5 Transparent Covering:

During the thermal operation of a flat solar collector, the transparent covering plays an essential role, which is to enable the greenhouse effect: it must transmit as much as possible of the incident solar radiation and absorb (or reflect in the case of so-called selective transparent coverings) the infrared rays coming from the absorber. It must also confine a layer of air above the absorber to limit convective exchanges. Paradoxically, the transparent covering is therefore responsible for the heating of the absorber due to the greenhouse effect, and through the re-emission of infrared rays, it becomes the site of the most significant thermal losses of the solar collector.

Its essential properties will thus be its optical characteristics and its mechanical resistance. They must exhibit a high energy transmission factor from 0.3 to 2.2 microns, i.e., across the solar spectrum, and a total opacity to far-infrared, from 4 to 30 μ, corresponding to the wavelengths of emission of the black body corresponding to temperatures from 100 °C to -20 °C (considering the width of the spectra). Furthermore, they must have good resistance to shocks and mechanical stresses, which can be caused by pressure variations or simple differential expansions.

Glass is generally chosen for solar collector coverings due to its optical properties. However, its shock resistance can only be ensured in operation by a high thickness (sometimes 4 to 6 mm) or special treatments (tempering). There remain two major drawbacks to the use of glass: its weight and the risks of accidental breakage during transportation, handling, or installation.

Therefore, many solar collector manufacturers are turning to the use of plastics, which are lighter and less fragile. However, while glass can be considered a reference material in terms of aging, the use of polymeric materials requires a serious study of their durability.

Currently, the three plastic materials used as coverings are:

• Polymethyl methacrylate (PMMA): a transparent thermoplastic sometimes called acrylic glass; chemically, it is the synthetic polymer of methyl methacrylate.

• Polycarbonate (PC),

• Polyester reinforced with glass fibers (GRP): GRP is a thermosetting composite material, mainly composed of unsaturated polyester resin, reinforced with glass fibers and filled with aggregates. The polyester resin acts as a binder between the different components.

These three materials are known and used in certain applications, particularly in the building sector for many years**.[10]**

| Matter | reflection | Thickness (mm) | transmittance λ=0.4÷2.5µm | transmittance ƒÉ=2.5€40ƒÊm | Cp (kJ/kg) | P (kg/m³) |
|---|---|---|---|---|---|---|
| Ferry | 1.518 | 3.175 | 0.840 | 0.702 | 0.754 | 2489 |
| fiberglass reinforced polyester | 1.540 | 6.350 | 0.870 | 0.076 | 1.465 | 1399 |
| Acrylicfiber (plexiglass) | 1.490 | 3.175 | 0.900 | 0.020 | 1.465 | 1189 |
| Polycarbonate (lexan) | 1.586 | 3.175 | 0.840 | 0.020 | 1.193 | 1199 |
| Polytetrafluoroethylene (teflon) | 1.343 | 5.080 | 0.960 | 0.0256 | 1.172 | 2480 |
| Fluorure de polyvinyle (Tedlar) | 1.460 | 1.016 | 0.920 | 0.07 | 1.256 | 137 |
| Polyester (mylar) | 1.460 | 1.270 | 0.870 | 0.178 | 1.046 | 1394 |
| fluoride polyvinylidene (Kynar) | 1.413 | 1.016 | 0.930 | 0.230 | 1.256 | 1770 |
| Polyethylene | 1.500 | 1.016 | 0.920 | 0.810 | 2.302 | 910 |

**Table II.2:**gathers the properties of various transparent surfaces **[11].**

**5.1. Transmission Factor:**

The transmission coefficient is the product of a coefficient related to the partial reflection of the incident radiation and a coefficient related to absorption within the transparent medium. This can be expressed as:

$$\tau = \tau_a, \tau_r \quad \textbf{(II.7)}$$

When radiation changes its propagation medium, it undergoes deviation upon passing through the interface, known as a dioptre, depending on the refractive index n of the medium (Figure II.3), according to Snell-Descartes' law **[12].**

$$n = \frac{n_2}{n_1} = \frac{\sin\theta_1}{\sin\theta_2} \quad \textbf{(II.8)}$$

Where n1 and n2 are the refractive indices and (\frac{n_1} {n_2} \) is the ratio between the refractive indices of the two media forming the interface.

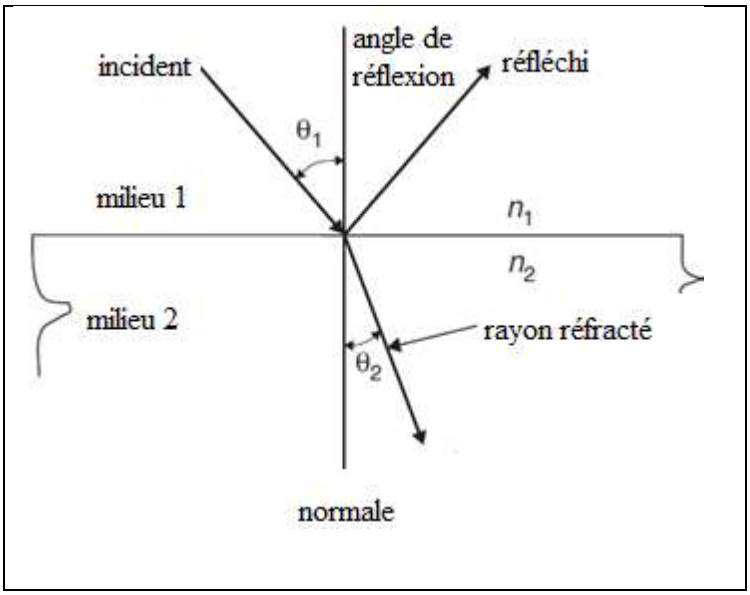


**Figure II.7:** Refraction of a light ray upon crossing a dioptre separating two media with different refractive indices.

The reflection coefficient can be determined by the **Fresnel formula [12]** in two components as follows:

$$r_1=[\frac{sin^2(\theta_2-\theta_1)}{sin^2(\theta_2-\theta_1)}] \quad \textbf{(II.9)}$$

$$r_2=[\frac{tan^2(\theta_2-\theta_1)}{tan^2(\theta_2-\theta_1)}] \quad \textbf{(II.10)}$$

$r_1$ : represents the perpendicular component of the reflected ray.

$r_2$: represents the parallel component of the reflected ray.

The properties are evaluated by calculating the average of these two components.

$$r =\frac{1}{2}(r_1+r_2) \quad \textbf{(II.11)}$$

For normal incident radiation, both angles are zero, hence:

$$r_0= (\frac{n_1-n_2}{n_1+n_2})^2 \quad \textbf{(II.12)}$$

Alternatively, if the medium (2) is air ($n_1 \approx 1$) and setting $n_1 = n$, this leads to writing:

$$r_0=(\frac{n-1}{n+1})^2$$

| Materials | Refractive index |
|---|---|
| Air | 1 |
| The water | 1.33 |
| Glass | 1.526 |
| Polycarbonate | 1.6 |
| Poly methacrylate | 1.45 |

**Table II.3:** Common Refractive Indices of Transparent Materials **[12, 13].**

Similarly, the transmission,$\tau_r$ (the subscript **r** indicates that optical losses due to reflection are taken into account), can be calculated from the average transmittance of the two components as follows:

$$\tau_r = \frac{1}{2}\left(\frac{1-r_1}{1+r_1} + \frac{1-r_1}{1+r_1}\right) \quad \textbf{(II.13)}$$

The transparent covering of a solar collector is generally made up of a parallel-sided slab, thus consisting of two interfaces that cause optical losses through reflection. For a ray of intensity equal to unity, a fraction (1 - r) penetrates into the material while a fraction is reflected. The transmitted part is reflected in turn and thus only transmits a fraction $(1 - r)^2$. And so on, the transmission coefficient **tp** is therefore written in accordance with Figure (II.9).

For a system with N coverings, we have **[12]:**

$$\tau_r = (1-\mathrm{r})^2 \sum_{n=0}^{\infty} \mathrm{r}^{2n} = \frac{1-\mathrm{r}}{1+\mathrm{r}} \quad \textbf{(II.14)}$$

The last expression becomes in the form:

$$\tau_r = \frac{1}{2}\left(\frac{1-r_1}{1+(2N-1)r_1} + \frac{1-r_1}{1+(2N-1)r_1}\right) \quad \textbf{(II.15)}$$

The transmission coefficient due to absorption of the medium is given by the following expression:

$$\tau_r - \frac{1}{2}\left(\frac{1-r}{1+(2N-1)r}\right) \quad \textbf{(II.16)}$$

The transmission coefficient due to absorption of the medium is given by the following expression:

$$\tau_a - \exp\left(-\frac{KL}{\cos\theta_2}\right) \quad \textbf{(II.17)}$$

Where K is the extinction coefficient (also called attenuation coefficient), which can vary from 4 $m^{-1}$ (for low-quality glass) to 32 $m^{-1}$ (for high-quality glass), and L is the thickness of the glass **[32].**

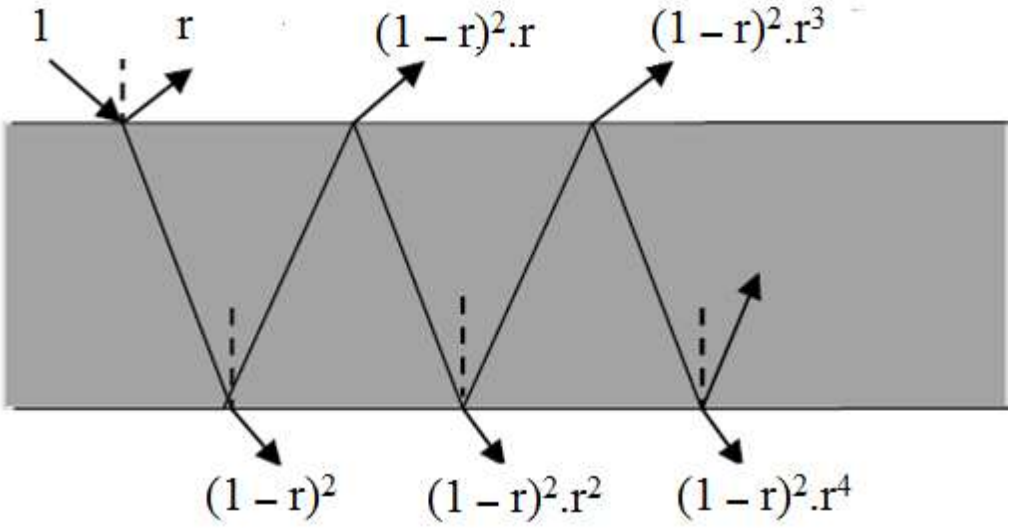


**Figure II.8:**Effect of multiple reflections on the transmission factor of a glass**.**

| Materials | Extinction coefficient |
|---|---|
| Solar glass | 4 |
| Window glass | 30 |
| Absorbent sun protection glass | 130÷270 |

**Table II.4:** Extinction coefficients of certain transparent materials **[13].**

## II.6 Heat Transfer Fluid :

To dissipate the heat stored by the absorber surface, either water or air is commonly used. The latter is distinguished by the following advantages:

• No freezing issues in winter or boiling in summer.

• With dry air, there are no corrosion problems.

• Simple implementation.

• Reliable system.

However, its use entails the following disadvantages:

• Air can only be used for space heating.

• The product of density by specific heat is low for air compared to water.

• Pipes must have a large cross-section to allow sufficient flow considering the previous remark.

• Thermal transfers are less effective than with water. In the case of pipes welded to the back of the absorber plate, care must be taken with the welds to minimize the thermal contact resistance as much as possible.

## II.7 The Insulator:

To minimize heat losses from the system, its walls need to be insulated. Towards the front, it is often an air gap that serves as insulation. Its thickness should not be too significant to limit convection transfers. A distance between 2 to 3 cm is typically chosen. At the rear part, one or more layers of insulation are placed, such as glass wool, polystyrene, or polyurethane foam; Table II.7 summarizes the main thermal properties of some insulating materials.

| Material | Thermal conductivity | Massicheat | Volumic mass | Diffusivity |
|---|---|---|---|---|
| Glass wool | 0.036 | 840 | 40 | 10.7 |
| Expandedpolystyrene | 0.040 | 1500 | 20 | 13.3 |
| Rockwool | 0.040 | 840 | 40 | 11.9 |
| Wool (clothing) | 0.040 | 1880 | 450 | 0.47 |
| Expandedcork | 0.048 | 1380 | 120 | 2.9 |
| Wood from Spain | 0.144 | 272 | 535 | 9.9 |
| Pure rubber | 0.153 | 2170 | 1200 | 0.6 |

**Table II.5:** Thermal Properties of Some Insulating Materials **[14].**

The study of solar collectors requires us to approach the modeling of incident radiation on an inclined plane at an angle beta with the horizontal.

## II.8 Passive Solar Design :

Passive solar design entails harnessing the radiant energy of the sun to regulate the thermal conditions within architectural spaces, encompassing both heating and cooling functionalities through strategic solar exposure. When sunlight interacts with a building structure, various mechanisms come into play wherein building materials may reflect, transmit, or absorb solar radiation. Moreover, solar-induced thermal gradients induce airflow patterns within designated spaces, offering a degree of predictability in environmental control. These fundamental responses to solar irradiance inform architectural considerations, material selections, and spatial arrangements conducive to leveraging solar energy for thermal regulation within residential contexts.

Diverging from active solar heating arrangements, passive systems are distinguished by their inherent simplicity, eschewing extensive reliance on mechanical or electrical apparatuses such as pumps, fans, or sophisticated control mechanisms for solar energy manipulation.**[15]**

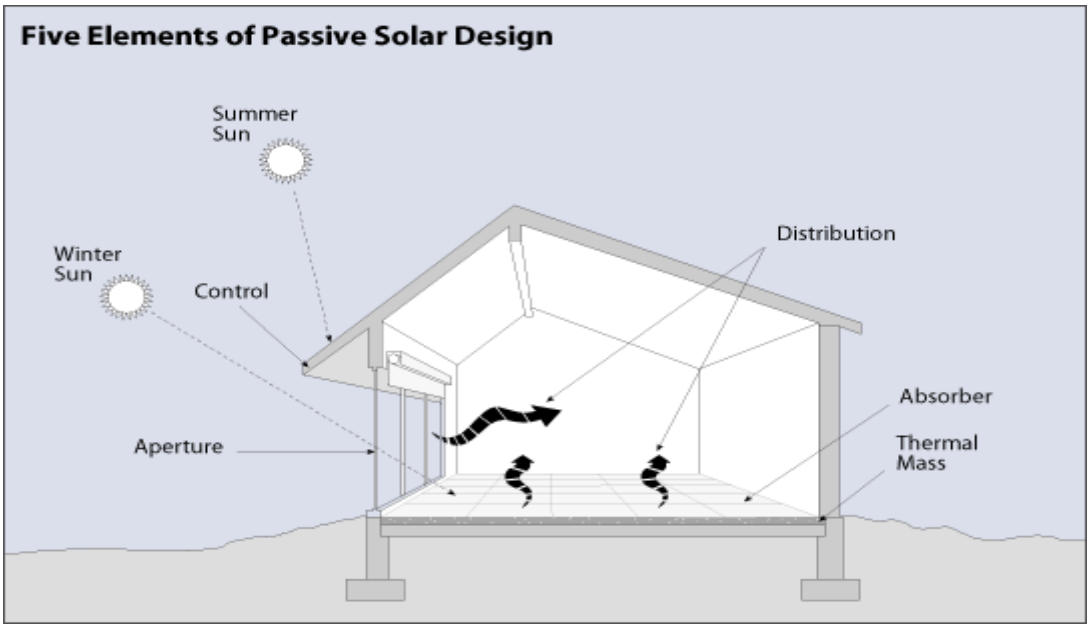


**Figure II.9.**Schema of passive solar design.

## II.9 active solar energy systems :

Active solar energy systems serve as invaluable allies in energy harnessing endeavors. These systems transcend mere absorption of sunlight, actively converting it into electricity capable of sustaining daily activities.

Comprised of essential components such as solar panels, inverters, and batteries, active solar energy systems operate collaboratively to capture, convert, and store solar energy. Diverging from their passive counterparts, active systems possess the capacity to generate electrical power, facilitating the operation of household appliances, electronic devices, and even electric vehicles.

Analogous to the process of making tea, active solar energy resembles the utilization of an electric kettle. Through active engagement with electricity, it swiftly heats water. Similarly, active solar systems leverage machinery such as solar panels and pumps to efficiently collect and distribute solar energy.

In contrast, passive solar energy mirrors the act of placing a teapot in a sunlit spot on a windowsill. Absent the need for specialized equipment or external power sources, passive systems rely on natural elements like windows and building materials to harness solar energy, gradually warming enclosed spaces without additional technological interventions.

Thus, while active solar energy necessitates electrical inputs and mechanical components akin to the electric kettle, passive solar energy operates organically, akin to the sun-warmed teapot. Each approach finds relevance contingent upon contextual considerations.

The adoption of an active solar setup confers a departure from exclusive reliance on conventional energy sources, potentially relegating burdensome utility expenses to obsolescence.

The allure of active solar energy resides in its capacity to furnish a sustainable remedy to escalating energy expenditures. Once operational, these systems avail themselves of the sun's boundless energy reservoir, culminating in diminished electricity bills and prospective long-term financial savings. In this symbiotic relationship between fiscal prudence and environmental stewardship, both economic interests and ecological imperatives converge harmoniously.**[16]**

## II.11 Conclusion

In this chapter, we have discussed the astronomical position of the sun and all aspects related to its internal structure. Additionally, we have examined the relationship between the Earth and the sun.

## II.11 References

[1] ÉCRIN (France). (2007). *Énergies alternatives*. Omniscience.

[2] D. K. Edwards, Capteurs solaires. Edition SCM, Paris. (1979).

[3] Sen Z. (2008). *Solar energy fundamentals and modeling techniques: atmosphere, environment, climate change and renewable energy*. Springer Science & Business Media.

[4] Salima K. (2009). *Etude théorique et numérique des systèmes couplés: distillateur plan capteur et distillateur hot box-capteur*. *Mémoire de magister UniversiteMentouri de Constantine*..

[5] Benbouza N. (2008). *Etude du rayonnement solaire dans la région de Batna* (Doctoral dissertation, Université de Batna 2).

[6] Bernard J. (2011). *Energie solaire: calculs et optimisation*. Ellipses.

[7] Faiza Merad. (2012). Magister en Physique.

[8] Nadjib R. Amélioration du chauffage solaire par l'addition des chicanes sous forme rectangulaire et transversal au sens d'écoulement de fluide.

[9] Merahi R, Chenni, R. (2018). *Nouvelles architectures distribuées de gestion et de conversion de l'énergie pour les applications photovoltaïques* (Doctoral dissertation, Université Frères Mentouri-Constantine 1).

[10] Aubert A. (1981). *Mesure du facteur d'émission des surfaces sélectives pour la conversion thermique de l'énergie solaire*. *Le Journal de Physique Colloques*, *42*(C1), C1-383.

[11] Garg H. P. (2000). *Solar energy: fundamentals and applications*. Tata McGraw-Hill Education.

[12] Kalogirou S. A. (2023). *Solar energy engineering: processes and systems*. Elsevier.

[13] Granqvist C. G. (2003). *Solar energy materials. Advanced Materials*, *15*(21), 1789-1803.

[14] Boutriaa A., &Chaker, A. (2009). Effet des paramètres de fonctionnement sur les performances d'un distillateur solaire.

[15]https://www.bigdogsolar.com/solar-school/what-is-active-solar-energy.ViewedDay 23/04/2024 by Hour 10:22.

[16]https://www.bigdogsolar.com/solar-school/what-is-active-solar-energy.ViewedDay 23/04/2024 by Hour 10:22 .

# CHAPTER III:

# EXPERIMENTAL STUDY

## III.1 Introduction

This scientific research focuses on solar thermal collectors, a widely known technology. Contemporary academic discourse and research endeavors are increasingly directed towards this area, with the primary aim and purpose of enhancing the effectiveness of these collectors. Our research, conducted between February and May 2024, included experiments on a restored solar thermal collector within the technological facilities of the Department of Mechanical Engineering of the University of Biskra. The collector is positioned at a 38° angle to the south and consists of a single-pass insulator featuring a glass cover with a transmission coefficient (τ) of 0.9. The absorber is made of galvanized steel, has a coefficient (α) of 0.95 and emissivity (ε) of 0.95. The collector accommodates a moving air stream with a height of 40 mm and is mounted on a chassis to maintain a constant inclination relative to the horizontal plane.

### III.1.1 Thermal efficiency:

The thermal efficiency (η) is expressed by the following mathematical expression:

$$\eta = \frac{Qu}{(G \times S)} \qquad \textbf{(III.1)}$$

$Q_u$**:** The useful power

G : Solar radiation

S: the surface of the collector plate ($m^2$)

$$Q_u: A \times C_p \times (T_{outlet} - T_{inlet}) \qquad \textbf{(III.2)}$$

$$m = V \times A$$

Pressure drop :

$$\Delta p = \wedge \times \frac{L}{Dh} \times \frac{V^2}{2g} \qquad \textbf{(III.3)}$$

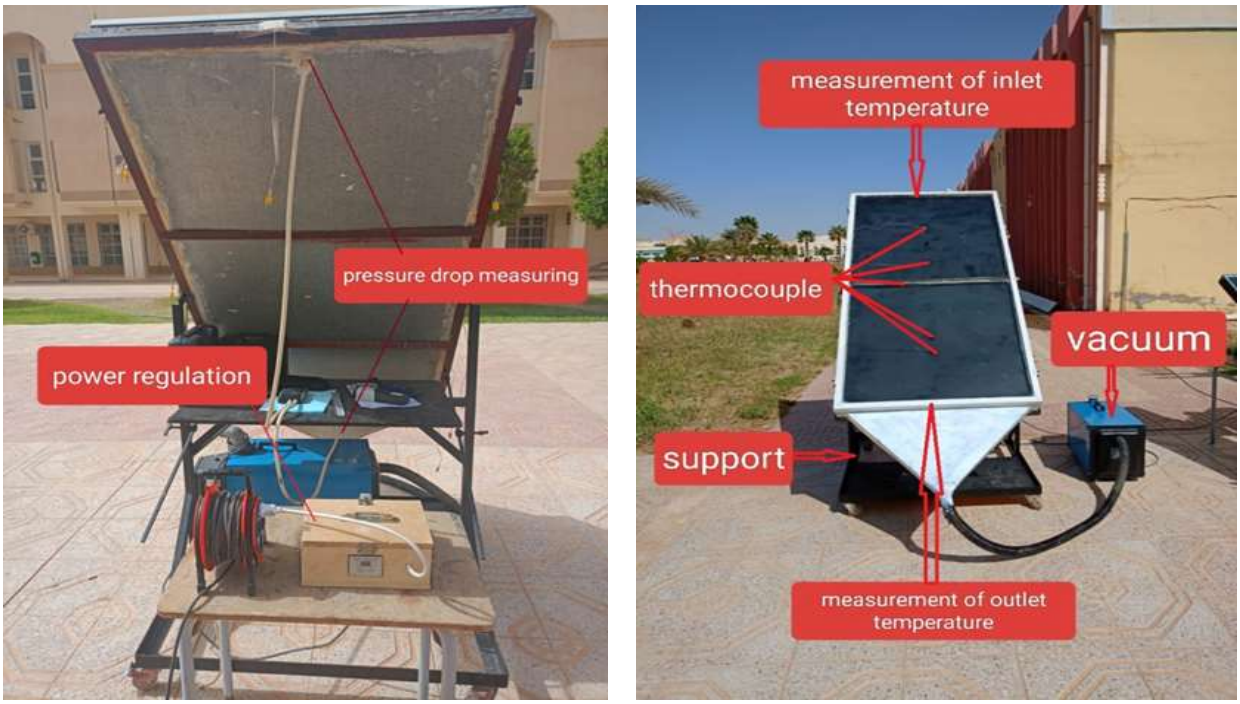


**Figure III. 1:** Experimental setup.

Figure 3.1 represents the experimental setup of the solar collectors, next to the technology hall of Mechanical engineering.

## III.2 Experimental apparatus:

### III.2.1 Description of the test ben:

The experiment was conducted in proximity to the technological facility of the Department of Mechanical Engineering at Biskra University, situated in the eastern-southern region of the Algerian Sahara, with geographic coordinates corresponding to a latitude of 34.5043°, a longitude of 5.4449°, and an elevation of 107 meters above sea level, as illustrated in (Figure III.2).


**Figure III. 2:** The experiment site “Google Earth”.

The focused research aims to enhance the thermal efficiency of the solar energy collector by implementing four modes, where the first mode did not add barriers, the second and third mode in which pyramid-shaped barriers of different arrangement were added, and the fourth mode in which pyramidal and rectangular barriers were added together within the flow channel of the solar energy collector. As shown in (Figure III.3).

Before the measurement procedures, the solar collector was removed one day before each position to facilitate the installation of barriers. On the day of measurement, the collector was oriented south and set at an inclination of 38°. A vacuum connection was established with the air outlet of the solar collector which in turn was connected to a voltage regulator to determine the mass flow rate. Measurements were then performed at 30-minute intervals.

The solar collector study is organized around four distinct operating modes:

- (Mode 1): smoothie plate (**SP**)
- (Mode 2): pyramide fins 1 (**PF1**)
- (Mode 3): pyramide fins 2 (**PF2**)
- (Mode 4) : pyramide rectangle baffles (**PRF**)

Each operational mode lasts for three days, starting at 7:00 a.m. and ending at 3:00 p.m. The flow rate started on the first day at 0.014 kg/s, increased to 0.024 kg/s on the second day, and increased to 0.033 kg/s on the third day. However, progress has been hindered

The study was postponed due to weather conditions, especially sudden cloud cover, which led to the disruption of operations.


**Figure III. 3:** Different types of modes studied.

### III.2.2 Technical characteristics:

The main components of the collector consist of:

- A transparent Plexiglas cover with a thickness of 3mm.
- A thin galvanized steel plate painted with black matte, fixed within a wooden frame.
- Two wooden supports affixed on both sides of the airflow stream to secure the baffles, ensuring they do not make direct contact with the absorber surface on the upper side, while remaining separate from the insulating layer on the lower side.
- Insulation provided by a 40mm thick sheet of polystyrene.
- The entire assembly is housed within a metallic steel case.

**a. Components and dimensions :**

**Table III. 1 :** Dimensions of constituants**.**

| Building elements | Length(m) | Width(m) | Thickness(mm) |
|---|---|---|---|
| **Transparent cover** | 1,94 | 0,94 | 3 |
| **Absorber** | 1,94 | 0,94 | 0,8 |
| **Wood frame** | 2 | 1 | 30×30 |
| **Wood sticks** | 1,94 | 0,03 | 30 |
| **Insulating** | 2 | 1 | 40 |
| **Case** | 2 | 1 | 80 |
| **Baffles pyramide** | 0,037 | 0,037 | 2 |
| **Baffles rectangle** | 0,88 | 2cm | 1,2 |

**b. Thermo-physicalcharacteristic :**

**Table III. 2:** Thermo-physical characteristics of the components.

| Elements | Materials | ρ(kg/m$^3$) | Cp (J/kg.K) | λ(w/m.K) |
|---|---|---|---|---|
| **Transparent cover** | Plexiglas | 1.2 | 1500 | 1.5 |
| **Absorber** | Galvanizedsteel | 7800 | 473 | 45 |
| **Wood frame** | Wood | 5100 | 1200 | 0.15 |
| **Wood sticks** | Wood | 5100 | 1200 | 0.15 |
| **Insulating** | Expandedpolystyrene | 16 | 1670 | 0.037 |
| **Case** | Galvanizedsteel | 7800 | 473 | 45 |

**c. Optical characteristics :**

**Table III. 3:** Optical characteristics of the building elements.

| Elements | Emissivity(ε) | Absorption (α) | Transmission(τ) |
|---|---|---|---|
| **Transparent cover** | 0,9 | 0,05 | 0,9 |
| **Black painted Absorber** | 0,95 | 0,9 | - |
| **Insulating** | 0,6 | 0,14 | - |
| **Case** | 0,89 | 0,8 | - |
| **Baffles pyramide** | 0,89 | 0,8 | - |
| **Baffles rectangle** | 0,89 | 0,8 | - |

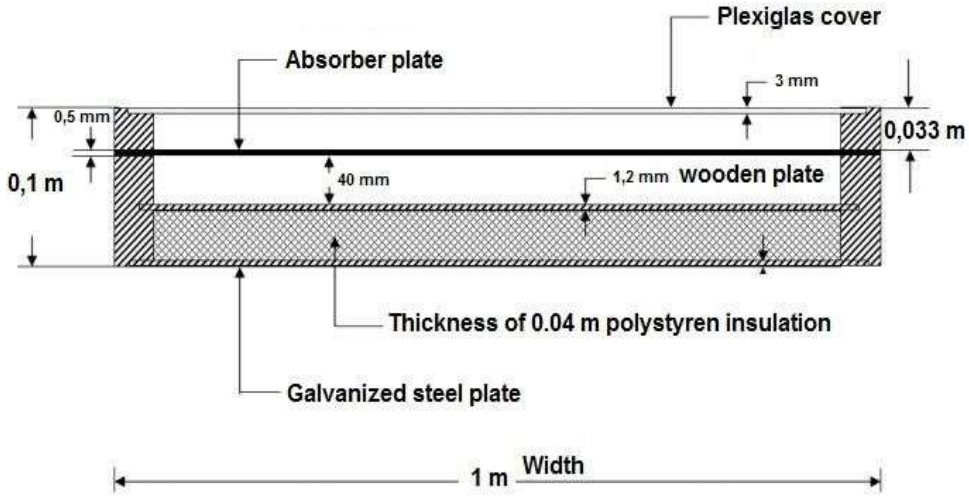


**Figure III. 4:** Characteristics dimensions.

- **Characteristics dimensions:**

The designed solar energy collector consists of glass, with an absorber underneath it, and beneath this absorber is a vacuum consisting of pyramidal barriers oriented at an angle of (180) with the addition of rectangular barriers at an angle of (45), and the barriers have fixed distances between them, and the air flows in this collector with a vacuum of (40 mm). The distance between the material the pipette and the glass cover (30 mm) (length = 0.94 m. width = 0.02 m. height = 0.08 mm). This layout was chosen because it turned out to be the optimal configuration. The number of sections was chosen and distributed according to the studied locations, and a vacuum was installed at the sensor outlet. To absorb heat transfer fluid (air).

- **Shape and arrangement of baffles:**

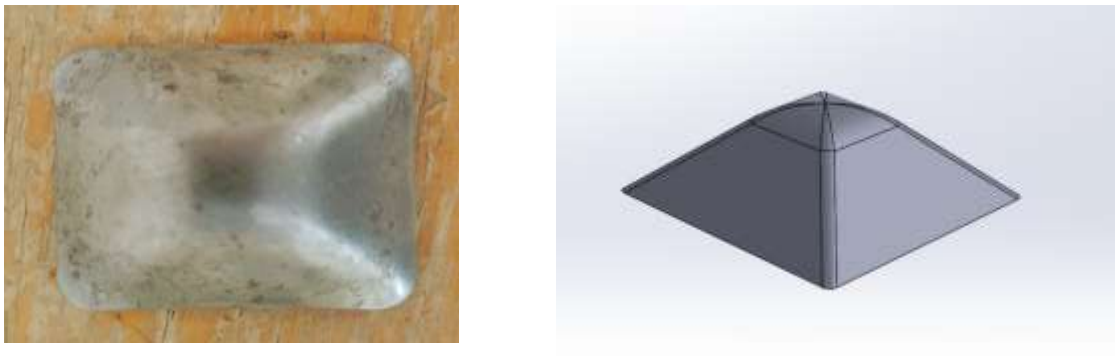

**Figure III. 5:** Pyramid Baffle.

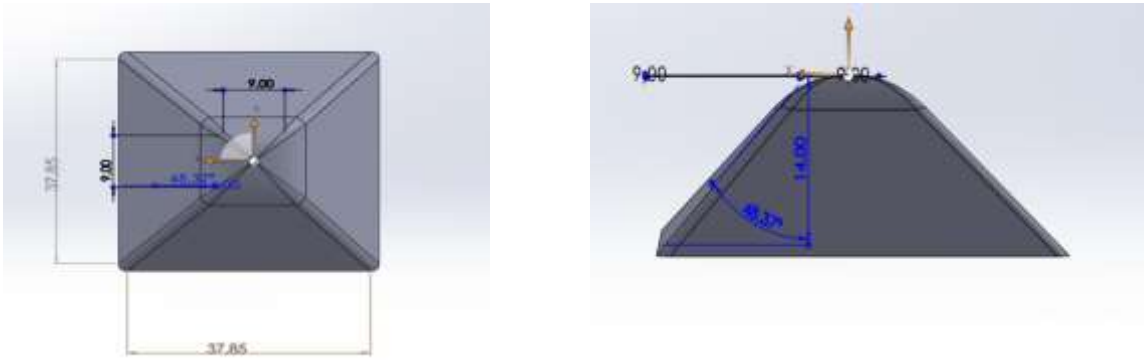


**Figure III.6:** Mesurement of dimensions Pyramide Baffles.

**Figure III. 7:** The baffles shape rectangle.

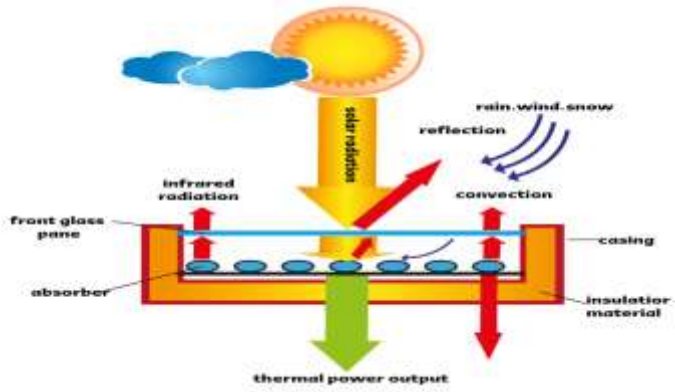


**Figure III. 8:** Principle of operation of solar collectors.

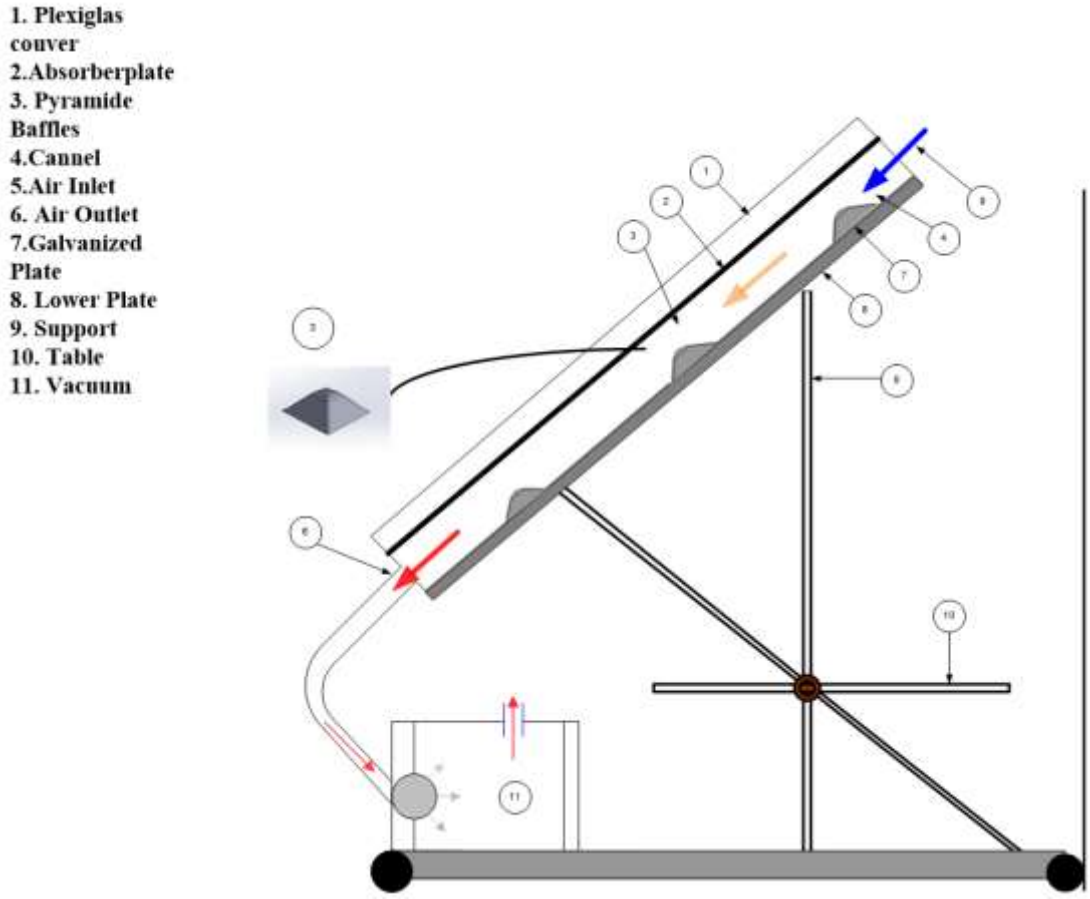


**Figure III. 9:** Schema of the solar collector With Baffles.

### III.2.3 Test Preparation:

 Experimental determination of the surface area of the solar collector:

- The dimensions of the solar collector are as follows:

  - Overall dimensions: 2m × 1m.

  - Opening dimensions: 1.88m × 0.88m.

- Surface calculation:

  - Total surface area: 2m².

  - Opening surface area: 1.66m².

 Experimental conditioning:

Before conducting the tests, the following preparations were carried out:

- The inclination angle of the collector was set to 38° facing south.

- A thorough inspection of the collector was performed to identify any damage or irregularities.

- The collector cover was meticulously cleaned to ensure optimal transparency.

- The collector was positioned under clear, cloudless conditions.

- The actual performance characteristics of the collector were determined.

- The flow rate was stabilized for consistent experimental conditions.

### III.2.4 Measuring instruments:

My investigation of the solar collector relied on employing various instruments for measuring temperature, solar radiation, pressure drop, wind speed, and the flow rate of absorbed fluid.

**● Voltage regulator:**

A voltage regulator serves as a pivotal component within the power supply unit, guaranteeing a consistent and stable voltage output across all operational scenarios. Its function encompasses regulating both mass flow and voltage levels amidst fluctuations in power supply and variations in load conditions. Remarkably, it possesses the capability to regulate both AC and DC voltages.

**Figure III. 10:** Voltage regulator.

**● Measurement of solar radiation:**

The instrument utilized for measuring solar radiation is specifically engineered for field assessments of global solar irradiance. Covering a spectrum ranging from approximately 300 to 2,800 nanometers, it provides accurate readings of solar radiation intensity. Equipped with a digital display, it facilitates direct visualization of irradiance values in watts per square meter ($W/m^2$).

Type:

**Figure III. 11:** Pyranometer for measuring solar irradiance.

Technical data :

- Dimensions : 185 x 108 x 56 mm.
- Power supply: 9V battery.
- Measuring range: 0-1999 W/m2.
- Resolution: 1 W/m2.
- Accuracy: +/-5% of full scale.

● **Flow Measurement:**

The wing-wheel thermo-anemometer serves the purpose of measuring air velocity, air temperature, and flow rate. Featuring the impeller PCE-TA 30, this thermo-anemometer enables instantaneous measurement with readings displayed on a large screen equipped with a backlight. Notably, the device facilitates the retention of current values on the screen while also indicating the maximum and minimum values recorded.

Type: Thermo-anemometer PCE-TA 30.

Technical data :

- Power supply: 9V battery.
- Dimensions :163 x 45 x 34 mm.
- Weight: 257 g.

- anemometer: 0 ºC ... +40 ºC / <95% H.R.
- thermal probe: 0 ºC ... +50 ºC / <80% H.R.


**Figure III. 12:** Flow measurements device.

● **Measurement of temperatures:**

Utilizing Thermocouple Sensor K type thermocouples, temperature measurements can be conducted within the range of -200°C to 1372°C (-328°F to 2501°F). Key characteristics of this sensor include:

- LCD display with backlight for enhanced visibility.

- Compatibility with K type Thermocouple input.

- Dual Thermocouple Input with capabilities for MaxHold and DataHold functionalities.

- Ability to measure temperature differentials (T1-T4).

- Option to select temperature units in user-preferred formats: °C, °F, or K.

- Power supply: 9V battery.

**Figure III. 13:** Thermocouple Sensor Type K.

● **Pressure drop measurement:**

The Differential Pressure Anemometer DM3 series is a dependable instrument designed for measuring gas pressure within the range of -2000 mbar to +2000 mbar, or from 1.5 m/s to 180 m/s (depending on the specific model). Capable of measuring both positive and negative pressure (vacuum), this device offers the following technical specifications:

- Pressure ranges from: 0/+20 Pa to -20,000/+20,000 Pa.

- Power supply: 9V battery.

- Operating temperature: 0 to +60°C.

- Storage temperature: -10 to +70°C.

- Dimensions: 155mm × 96mm × 28.2mm.

- Air velocity range: 1.5m/s to 18m/s.


**Figure III. 14:** Pressure Anemometer DM3 series.

● **Air circulation control:**

To regulate air circulation throughout the experiment, a mobile vacuum cleaner with a suction drive of 1 kW and a weight of 30 kg was employed.

Technical specifications include:

- Machine type: air filter.
- Manufacturer: AB Electrostatic.
- Model: MPF-803.
- Dimensions: depth 84cm, width 32.5cm, height 42.5cm.

**Figure III. 15:** Vacuum.

● **Measurement of humidity:**

The manual hygrometer presented here is specifically engineered for swift and accurate measurements of both temperature and humidity. Its compact design renders it particularly suitable for on-site applications.

Features include:

- Fast response time.
- High accuracy in measurement.
- Simultaneous indication of temperature and humidity.
- Automatic shutdown functionality.
- Calculation capabilities for dew point and wet bulb temperature.
- Backlight for enhanced visibility.
- Storage of maximum values.

- Compact and lightweight construction.

**Figure III. 16:** Hygro-thermometer PCE-555.

## III .3 Conclusion:

The conclusion drawn is that the research conducted on solar thermal collectors at the University of Biskra is a comprehensive study aimed at improving the efficiency of solar energy capture. The study meticulously details the experimental setup, including the design and characteristics of the solar collector, and the methodology for testing different configurations to optimize thermal efficiency. The research highlights the importance of precise measurements and controlled conditions to accurately assess the performance of the solar collector. It also underscores the potential of innovative designs, such as the use of pyramid and rectangular baffles, to enhance the collector's ability to harness solar energy. Overall, the study represents a significant step towards advancing solar thermal technology and its application in sustainable energy solutions.

# CHAPTERIV

# RESULTS AND DISCUSSIONS

## IV.1 Introduction

In this chapter, we will examine studies conducted by various scientists regarding solar energy collectors and assess their significance and impact.

## IV.2 Interpreting the results:

### IV.2.1 Solar radiation for each day of the experiments:

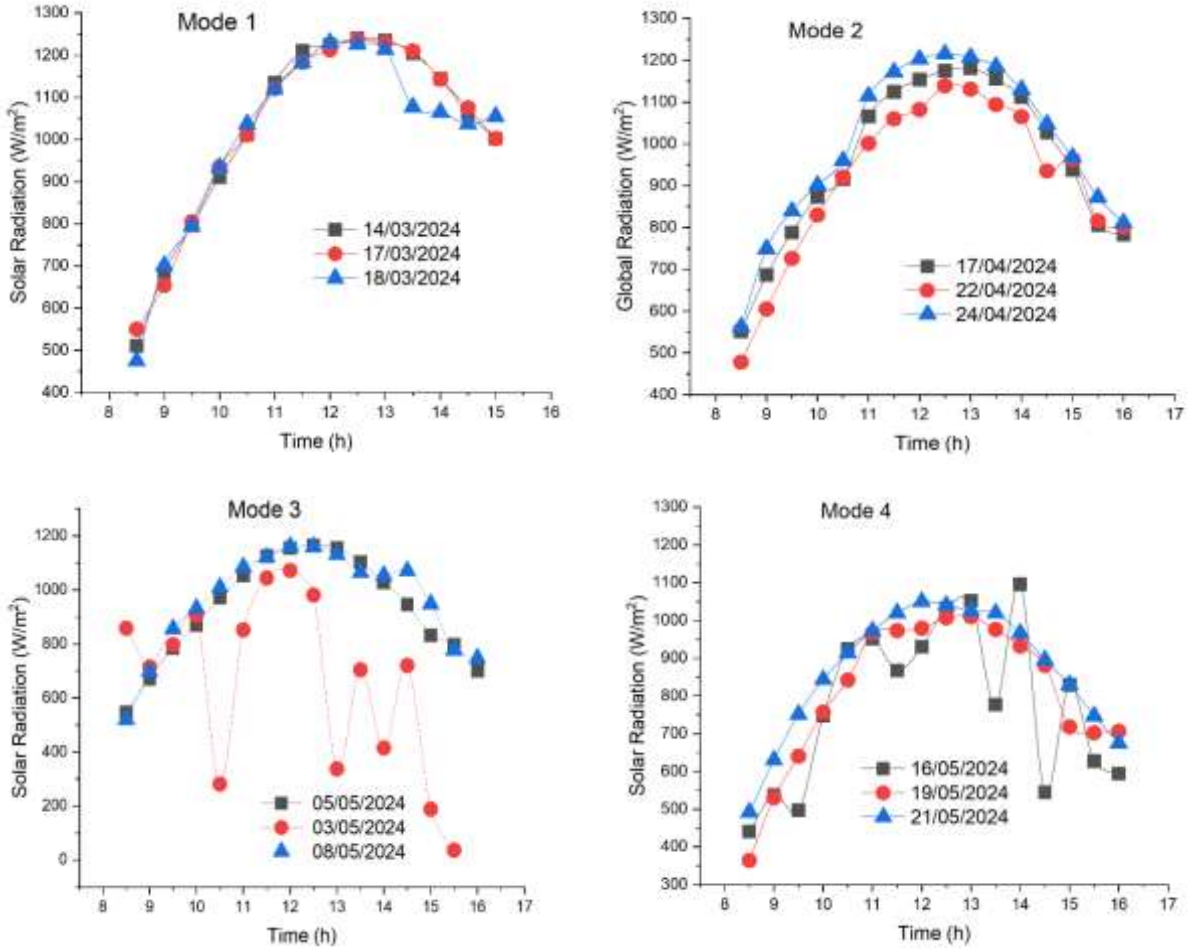


**Figure IV.1.** Global solar radiation versus the time of the day**.**

Figure IV.1 show the variation of the global solar radiation as a function to time of the day, according to different day and month Sach as March, April, and May. The study selected four modes of the solar collector with and without baffles that explain the four test of the figures in the one image.

The global solar radiation selected a maximum value in the midday which attain to 1300 w/s, and constatetoo the low values which touch approximation to the sunrise and sunset because estimated the slow value of the global solar radiation.

Sometimes we have seen some fluctuation of the global solar radiation, this irregular form of evolution back to nature of the climate which the sky effect directly on value of the global solar and this last effect has influence onto result of the thermal efficiency.

### IV.2.2 Wind Speed for each day of the experiments:

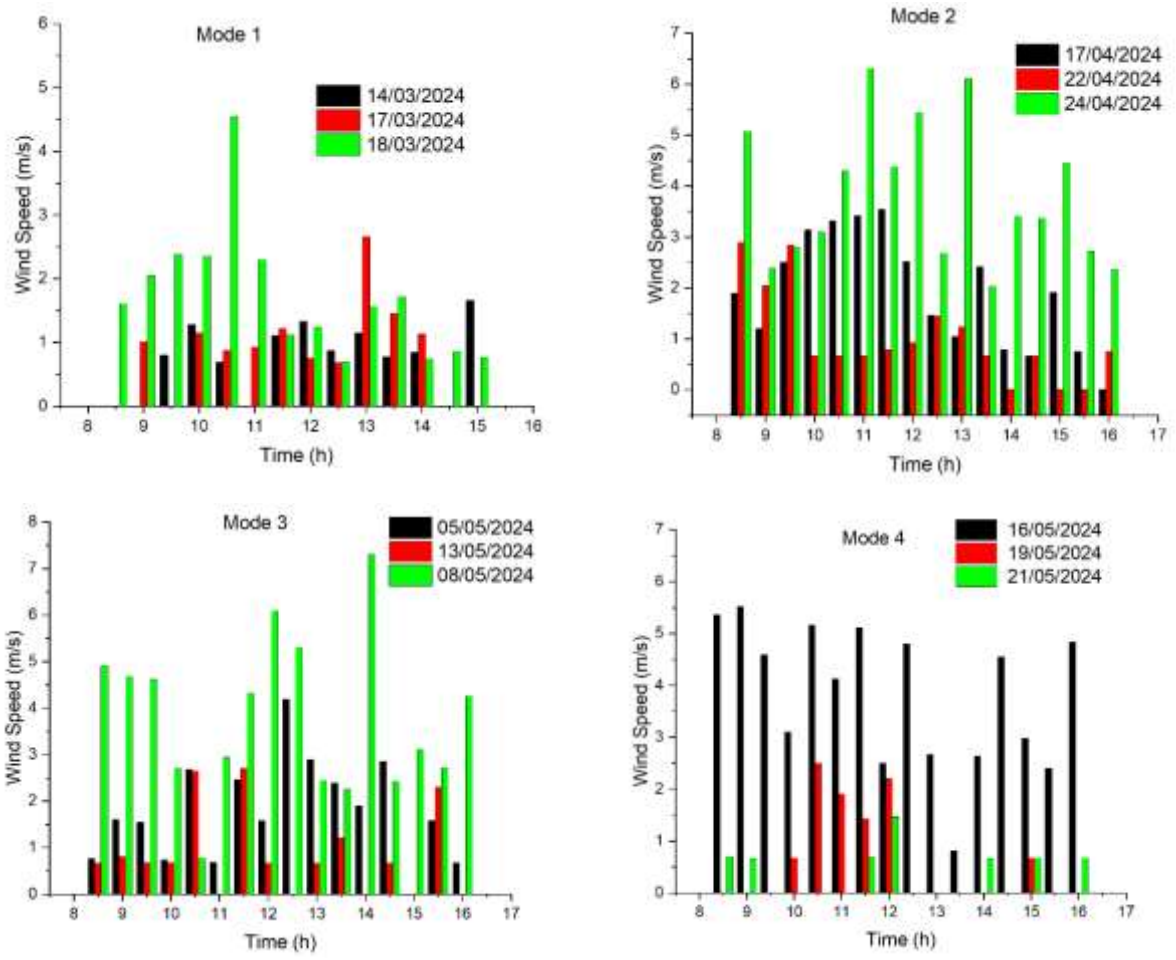


**Figure IV.2** Wind Speed for each day of the experiments.

Figure IV.2 show the variation of the wind speed as a function to time of the day, according to different day and month for each experimental study. We can be seen that the wind speed takes irregular form which effected for all parameters such as the temperature of an absorber plate, outlet temperature of the solar collector, and the thermal efficiency. This part of the evolution enters in the lost heat convection. We constate a maximum value which attain to 7.5 m/s corresponding to mode 3 according to third test of the experiment when mass flow rate equal to 0.033 kg/s.

### IV.2.3 Ambient Temperaturefor each day of the experiments:

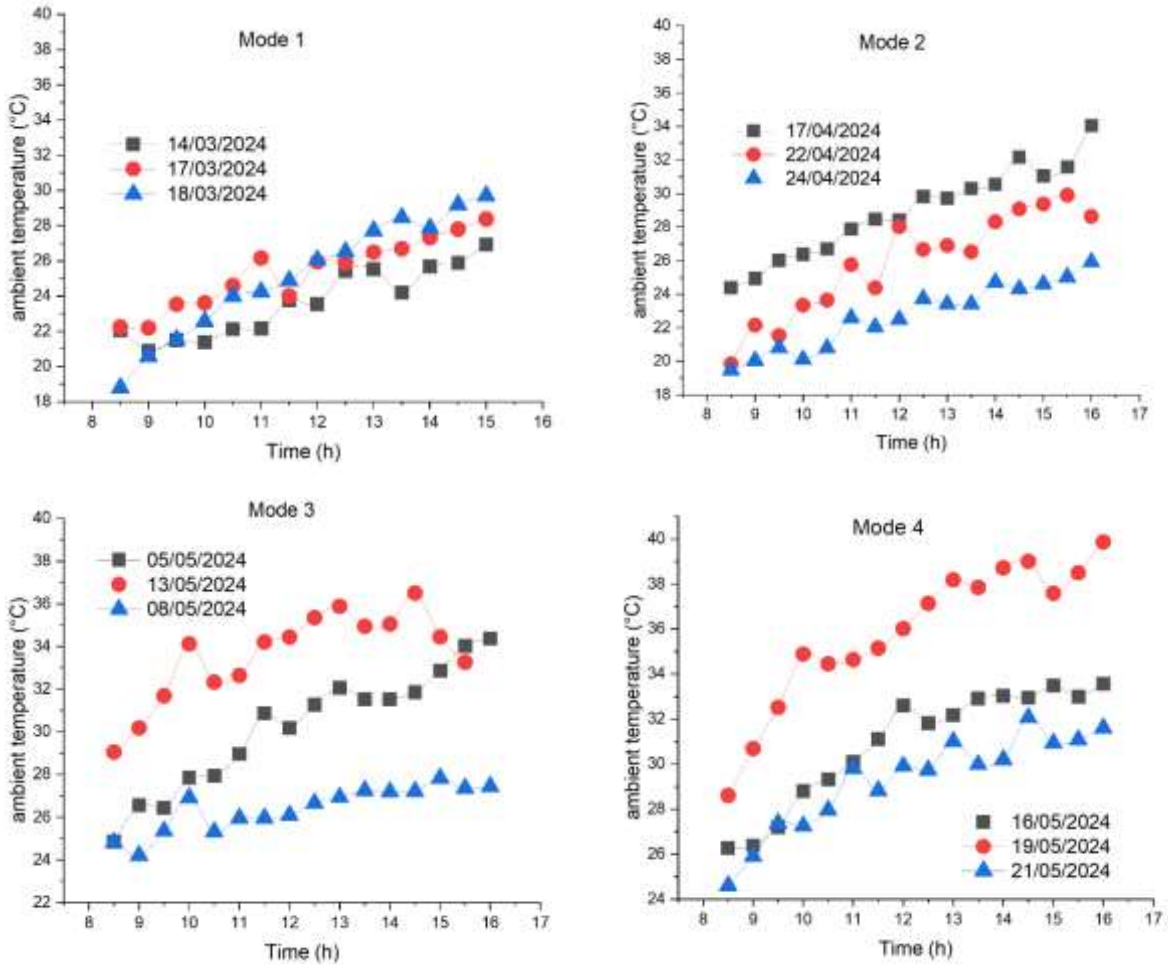


**Figure IV.3** Ambient Temperature for each day of the experiments.

Figure IV.3 represent the evolution of the ambient temperature as a function to time of the day, according to different days and month. The ambient temperature has a higher value in the day 9/05/2024 attain to 44°C, and low values about 24/04/2024 which attain to 26 °C. The ambient temperature estimated the important factor because it is entered in the solar collector with initial energy.

### IV.2.4 The differential temperature of the solar collector:

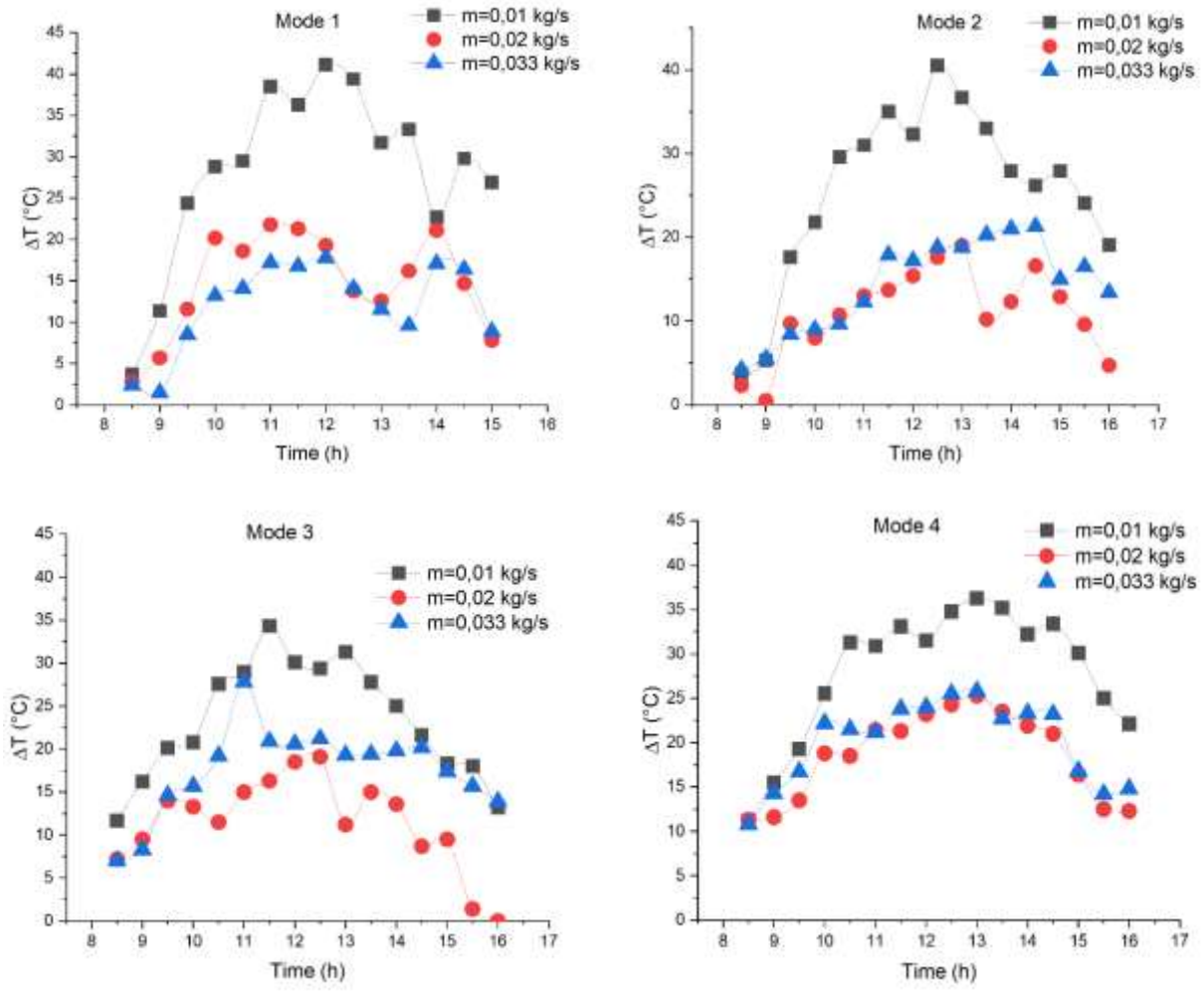


**Figure IV.4**Different Temperature corresponding to different modes.

The figure represents the difference in temperature between the inlet and outlet as a function of time of day for each mass flow rate. It is noticeable that at the beginning of the experiment study, the temperature difference start with low value, then continuity to increase successively to attain the value equal 43 °C at 12:00 corresponding to mode1, according to mass flow rate equal to 0.01 kg/s, while in the second mode, the difference temperature has reaches approximately to 40 °C at 12:30. In the third mode, the difference temperature reaches approximately 37 °C at 11:30, and in the last mode, the difference temperature reaches approximately 36 °C at 13:00. We can be observed where increase the mass flow rate, applied the temperature difference decreases.

### I.V.2.5 Pressure Variation for each day of the experiments:

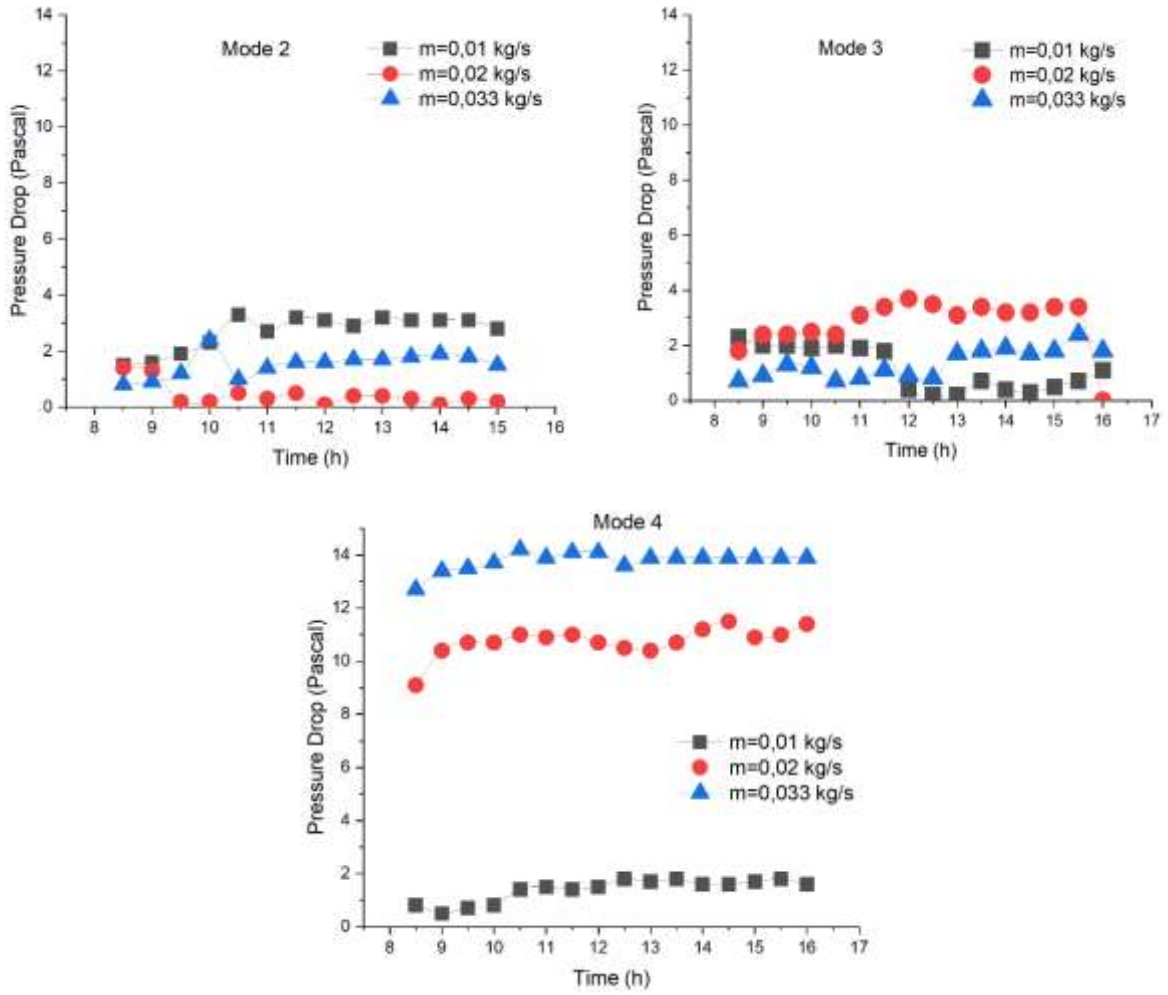


**Figure IV.5** Pressure Variation for each day of the experiments.

Figure IV.5 show the variation of the pressure drop as a function to time of the day. Conclude that the pressure drop effect by the mass flow rate in the parallel just in the mode 4, because we have the copulate between the pyramids and rectangular baffles.

### IV.2.6 Performance of the solar collector:

After an effort lasting three months, March, April, and May, we obtained the following results presented in Chapter Four of the thesis. Upon reviewing them, we concluded that integrating barriers significantly improves thermal efficiency. When evaluating the efficiency of the four barrier situations, it became evident that the fourth situation provides the best efficiency compared to the remaining situations.

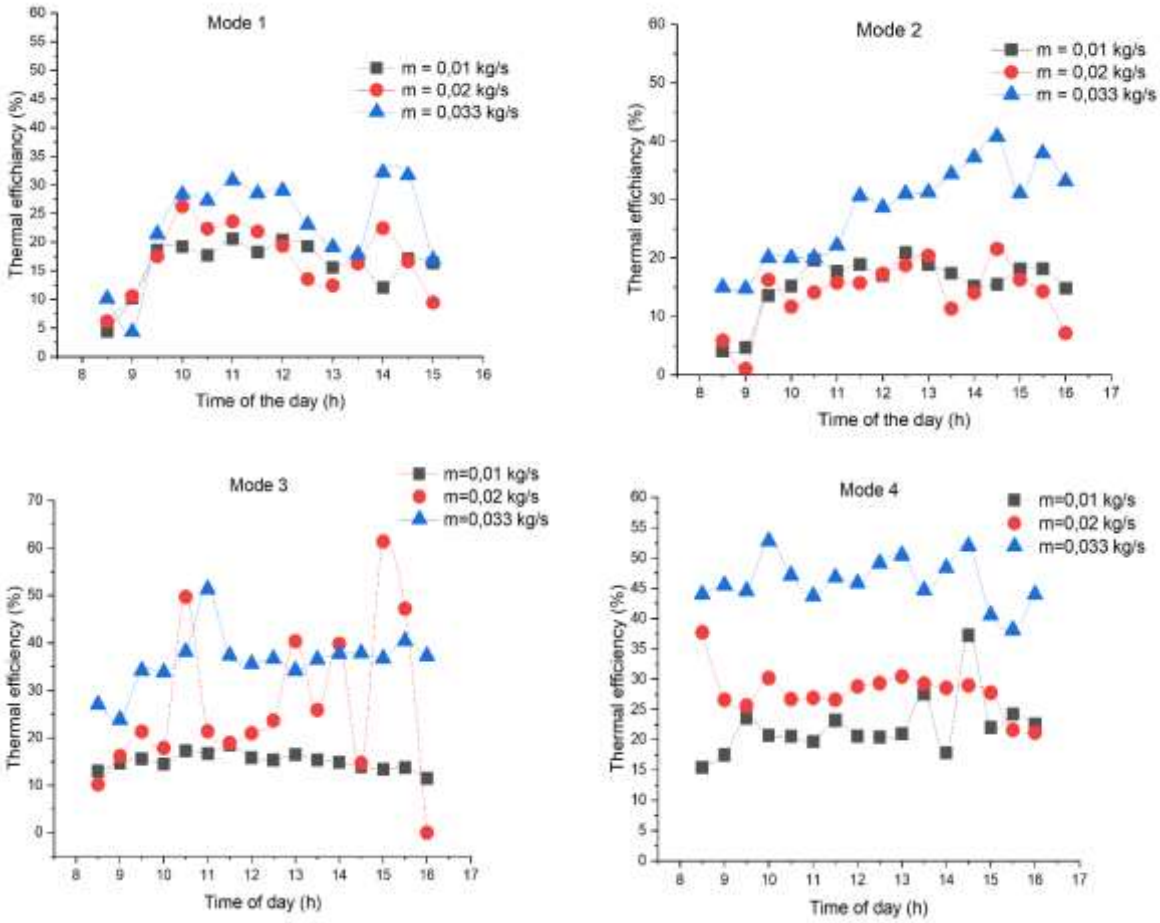


**Figure IV.6**Thermal efficiency versus time of the day.

### IV.2.7Local heat transfer by convection:

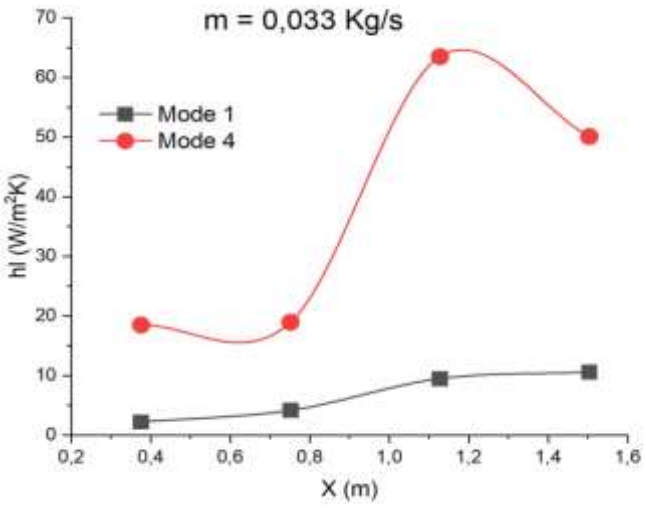


**Figure IV.7**local heat transfer by convection versus the longer solar collector.

Figure IV.7 shows local convective heat transfer versus solar collector length. Observations from the data indicate that the local heat transfer value inside the solar collector starts from a low value. Initially, at the inlet section of the solar collector, the hl is relatively low, ranging from 2 to 18 (W/m²K) along a length of 0.4 (m) see (Figure IV.7). However, as the collector length increases, there is a corresponding increase in the local heat transfer rate. This increase continues until it reaches a peak value of 63 (W/m²K) in the fourth mode.

In addition, it should be noted that the local heat transfer rate is affected by the fluid flow rate within the collector. Specifically, an increase in flow rate results in greater local heat transfer. This relationship can be attributed to enhanced convective heat transfer resulting from increased fluid velocity. A higher flow rate results in more robust fluid movement, which promotes better heat exchange between the solid and liquid surface, by obtaining higher local heat transfer rates.

**IV.2.8 Nusselt Number:**.

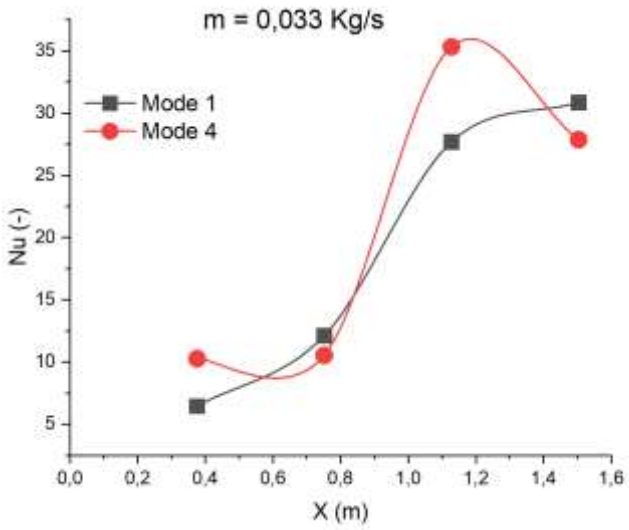


**Figure IV.8** Nusselt number versus length of the solar collector.

Figure IV.8 shows the Nusselt number versus the length of the solar collector. An in-depth analysis of the available data reveals a convincing and scientifically accurate behavior of NuL inside the solar collector between Mode 1 being without baffles and Mode 4 with mixed baffles. Initially, at the inlet section of the complex, NuL shows the relatively lowest values, which typically range between 2 and 10 along a length of 0.4 (m). As the length of the solar collector gradually increases, there is a distinct and steady upward trajectory in the NuL. It increases until it reaches its highest value, which is 35, during the fourth mode.

It is worth emphasizing the profound influence of fluid flow rate on the NuL inside the solar collector. As the flow rate of the fluid circulating inside the system becomes clear with respect to NuL. This close association stems from the increased convective heat transfer attributed to the condensed fluid velocity. A higher flow rate results in more vigorous fluid movement, thus facilitating enhanced heat exchange between the solid and liquid surface. As a result, these intense fluid dynamics produce high NuL values, representing a more efficient heat transfer process.

## I.3. Conclusion

After reviewing the results and conducting a comprehensive comparison, it is evident that integrating barriers significantly improves thermal efficiency. Furthermore, when evaluating the efficiency of the three barrier-inclusive conditions compared to the condition without barriers, it becomes apparent that the latter outperforms the former in terms of efficiency. This conclusion is further supported by the results of the remaining cases, as detailed in this chapter.

# General Conclusion

# General Conclusion

In this experimental study, our aim was to investigate the impact of barrier integration on the thermal efficiency of a solar collector for air heating. The experiments were conducted within our dedicated facilities in the Department of Mechanical Engineering at the University of Biskra.

We meticulously provided all constituent elements of the collector and the measurement tools used in our tests. Through precise control of experimental conditions, we sought to establish a reliable basis for assessing the effects of barriers on collector performance.

Our study focused on four distinct configurations of the solar energy collector, each corresponding to a different number of barriers: Configuration 1 without barriers, Configuration 2 with 90 baffles, Configuration 3 with 127 baffles, and Configuration 4, which involved a mixture of the latter configuration with an additional six rectangular baffles. Through comprehensive testing, we analyzed the thermal performance and efficiency for each configuration.

The results obtained from our experiments revealed the significant impact of baffles on collector efficiency. We noted that the addition of baffles not only led to an increase in overall efficiency but also shed light on the importance of their specific placement within the collector.

Furthermore, our findings indicated that introducing baffles resulted in increased turbulence within the collector, enhancing heat transfer between the absorber plate and the airflow beneath it. This improved heat exchange contributed to enhancing efficiency overall.

Regarding performance, we conclude that installing barriers across the entire airflow path yields greater efficiency (Configuration 4) compared to other configurations (Configuration 1, Configuration 2, Configuration 3), as observed in the figure. It also outperforms other configurations.

Overall, our study highlights the importance of integrating baffles into solar air heating collector systems to improve thermal efficiency. The specific configuration and placement of baffles play a crucial role in enhancing performance. By enhancing turbulence and heat transfer, the addition of baffles promises to achieve greater efficiency and overall performance in solar energy collection systems.